The formin FHOD1 and the small GTPase Rac1 promote vaccinia virus actin–based motility

Diego E. Alvarez and Hervé Agaisse

Department of Microbial Pathogenesis, Boyer Center for Molecular Medicine, Yale School of Medicine, New Haven, CT, 06519

Vaccinia virus dissemination relies on the N-WASP–ARP2/3 pathway, which mediates actin tail formation underneath cell-associated extracellular viruses (CEVs). Here, we uncover a previously unappreciated role for the formin FHOD1 and the small GTPase Rac1 in vaccinia actin tail formation. FHOD1 depletion decreased the number of CEVs forming actin tails and impaired the elongation rate of the formed actin tails. Recruitment of FHOD1 to actin tails relied on its GTPase binding domain in addition to its FH2 domain. In agreement with previous studies showing that FHOD1 is activated by the small GTPase Rac1, Rac1 was enriched and activated at the membrane surrounding actin tails. Rac1 depletion or expression of dominant-negative Rac1 phenocopied the effects of FHOD1 depletion and impaired the recruitment of FHOD1 to actin tails. FHOD1 overexpression rescued the actin tail formation defects observed in cells overexpressing dominant-negative Rac1. Altogether, our results indicate that, to display robust actin-based motility, vaccinia virus integrates the activity of the N-WASP–ARP2/3 and Rac1–FHOD1 pathways.
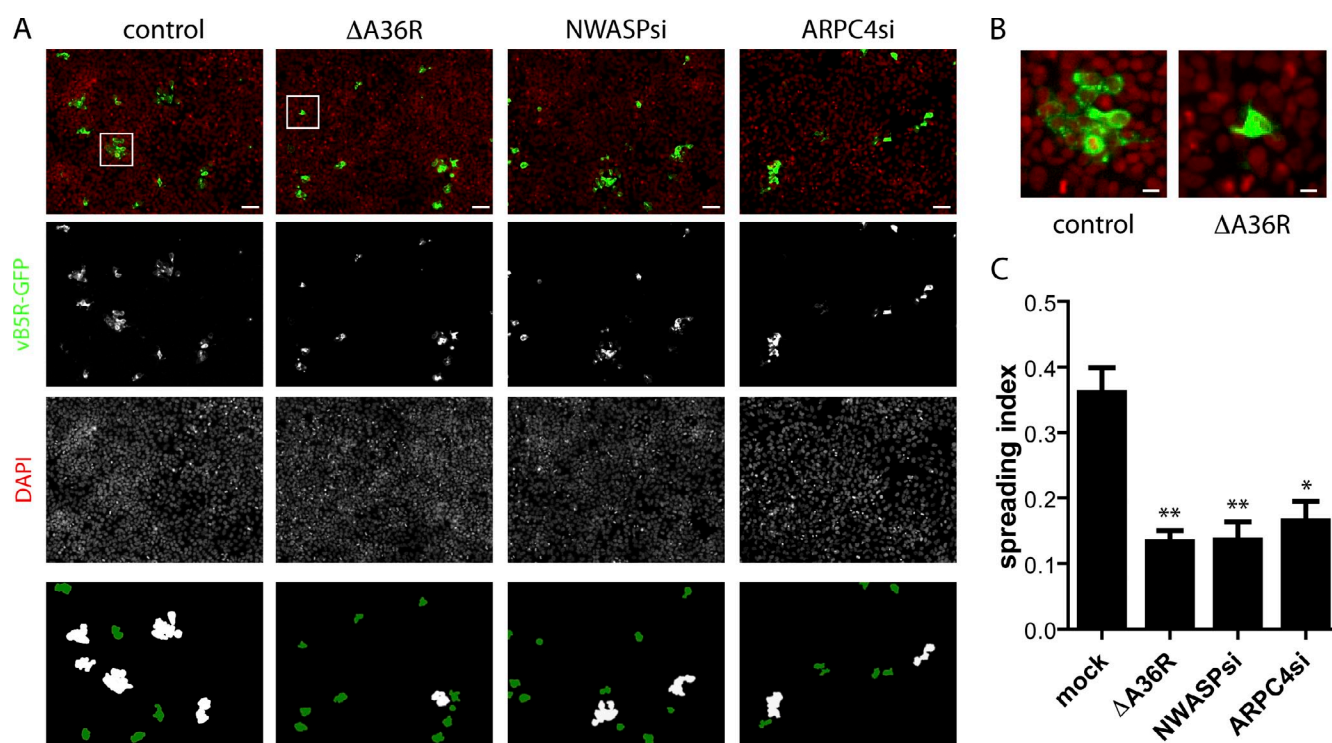
Introduction

The life cycle of *Orthopoxviruses*, such as vaccinia virus, relies on the dissemination of two infectious forms, the intracellular mature viruses (IMVs) and the extracellular viruses (EVs). IMVs propagate after massive release by cell lysis at the end of the infectious cycle. Vaccinia dissemination is also supported by the spread of EVs from cell to cell through actin-based motility (Smith et al., 2002; Roberts and Smith, 2008). The formation of EVs is complex and first requires wrapping of IMVs in double membranes derived from the trans-Golgi network or endosomes, leading to the production of intracellular enveloped viruses (IEVs; Hiller and Weber, 1985; Tooze et al., 1993; Schmelz et al., 1994). IEVs travel on microtubules and the fusion of their outer membrane to the plasma membrane leads to formation of cell-associated EVs (CEVs; Hollinshead et al., 2001; Rietdorf et al., 2001; Ward and Moss, 2001a; van Eijl et al., 2002). The viral proteins B5 and A36 are essential for vaccinia actin–based motility (Sanderson et al., 1998; Wolffe et al., 1998; Katz et al., 2003). B5 and A36 are located in the inner and outer membrane of IEVs, respectively (Engelstad et al., 1992; Isaacs et al., 1992; Parkinson and Smith, 1994; Röttger et al., 1999). The fusion of the outer membrane of IEVs

to the plasma membrane exposes B5 at the surface of CEVs (Engelstad et al., 1992; Isaacs et al., 1992) and positions A36 in the plasma membrane, underneath CEVs (van Eijl et al., 2000). The exact role of B5 in actin-based motility is unknown. The phosphorylation of the cytosolic tail of A36 by Src and Abl family members creates docking sites for the adaptor proteins Nck1 and Grb2 (Scaplehorn et al., 2002; Newsome et al., 2006). Nck1 and Grb2 mediate the recruitment of N-WASP, which mediates the recruitment and activation of the ARP2/3 complex (Frischknecht et al., 1999). The ARP2/3 complex binds existing mother actin filaments and nucleates the formation of daughter filaments that branch out from the mother filament leading to the formation of a branched network (Pollard and Borisy, 2003). The origin of the mother filaments required for initiation of ARP2/3-mediated actin polymerization is unknown. The assembly of actin beneath CEVs generates forces that drive the formation of virus-tipped membrane protrusions also referred to as actin tails, which leads to viral release into the extracellular environment or viral transmission to neighboring cells (Smith et al., 2002; Roberts and Smith, 2008).

Correspondence to H. Agaisee: herve.agaisse@yale.edu

Abbreviations used in this paper: CEV, cell-associated extracellular virus; DAD, diaphanous autoregulatory domain; EV, extracellular virus; GBD, GTPase binding domain; IEV, intracellular enveloped virus; IMV, intracellular mature virus; PBD, p21 binding domain; P-Src, phospho-Src.

The Rockefeller University Press $30.00
J. Cell Biol. Vol. 202 No. 7 1075–1090
www.jcb.org/cgi/doi/10.1083/jcb.201303055

JCB 1075

Figure 1. **Quantification of vaccinia virus spread from cell to cell.** (A) Spreading of vaccinia virus expressing a B5R-GFP chimera (vB5R-GFP) in HeLa cells at 16 h after infection. (control) Cells infected with wild-type virus. (ΔA36R) Cells infected with a vaccinia virus variant lacking A36R. (N-WASPsi) N-WASP–depleted cells infected with wild-type virus. (ARPC4si) ARPC4-depleted cells infected with wild-type virus. In N-WASP– and ARPC4-depleted cells, mRNA levels were consistently <20% of the levels observed in mock-treated cells. Top panels show representative images of HeLa cells (nuclei, red channel) infected with vaccinia virus (vB5R-GFP, green channel). Bars, 100 µm. Bottom panels display the corresponding image analysis showing large foci (white) and small foci (green). (B) Merged channels for the boxed areas in A showing representative foci of infection for cells infected with vB5R-GFP–expressing virus (control) or the variant lacking A36 (ΔA36R). Bars, 20 µm. (C) Graph showing quantitative analysis of cell-to-cell spread. The spreading index represents the ratio between the number of large foci and the total number of foci. Data are presented as the mean ± SD. *, P < 0.05; **, P < 0.01; P = 0.0015 for ΔA36; P = 0.0064 for NWASPsi; and P = 0.0120 for ARPC4si, compared with the control.

The manipulation of the actin cytoskeleton represents a common theme in pathogen dissemination. Similar to vaccinia virus, several bacterial pathogens, such as *Listeria monocytogenes* and *Shigella flexneri* also manipulate the ARP2/3 complex in order to spread from cell to cell. *L. monocytogenes* recruits and activates the ARP2/3 complex through ActA (Welch et al., 1998), a bacterial factor that mimics the activity of the nucleation-promoting factor N-WASP (Lasa et al., 1997; Skoble et al., 2000; Boujemaa-Paterski et al., 2001; Chong et al., 2009). In contrast, *S. flexneri* expresses a bacterial adaptor, IcsA, that mediates the recruitment of N-WASP, which then recruits and activates the ARP2/3 complex (Bernardini et al., 1989; Goldberg et al., 1994; Suzuki et al., 2002). On the basis of these investigations, pathogen dissemination was thought to rely solely on the manipulation of the ARP2/3 complex. However, Heindl et al. (2010) have recently reported that, in addition to manipulating the ARP2/3 complex for displaying cytosolic motility, *S. flexneri* requires formin family members for plasma membrane protrusion formation. Moreover, recent studies have unexpectedly revealed that *Rickettsia spp.* do not require the ARP2/3 complex to form actin tails and instead express and use the bacterial factor Sca2, a functional mimic of mammalian formins (Haglund et al., 2010; Kleba et al., 2010). Furthermore, a role for N-WASP recycling and clathrin-mediated endocytosis was recently reported in vaccinia actin–based motility (Weisswange et al., 2009;
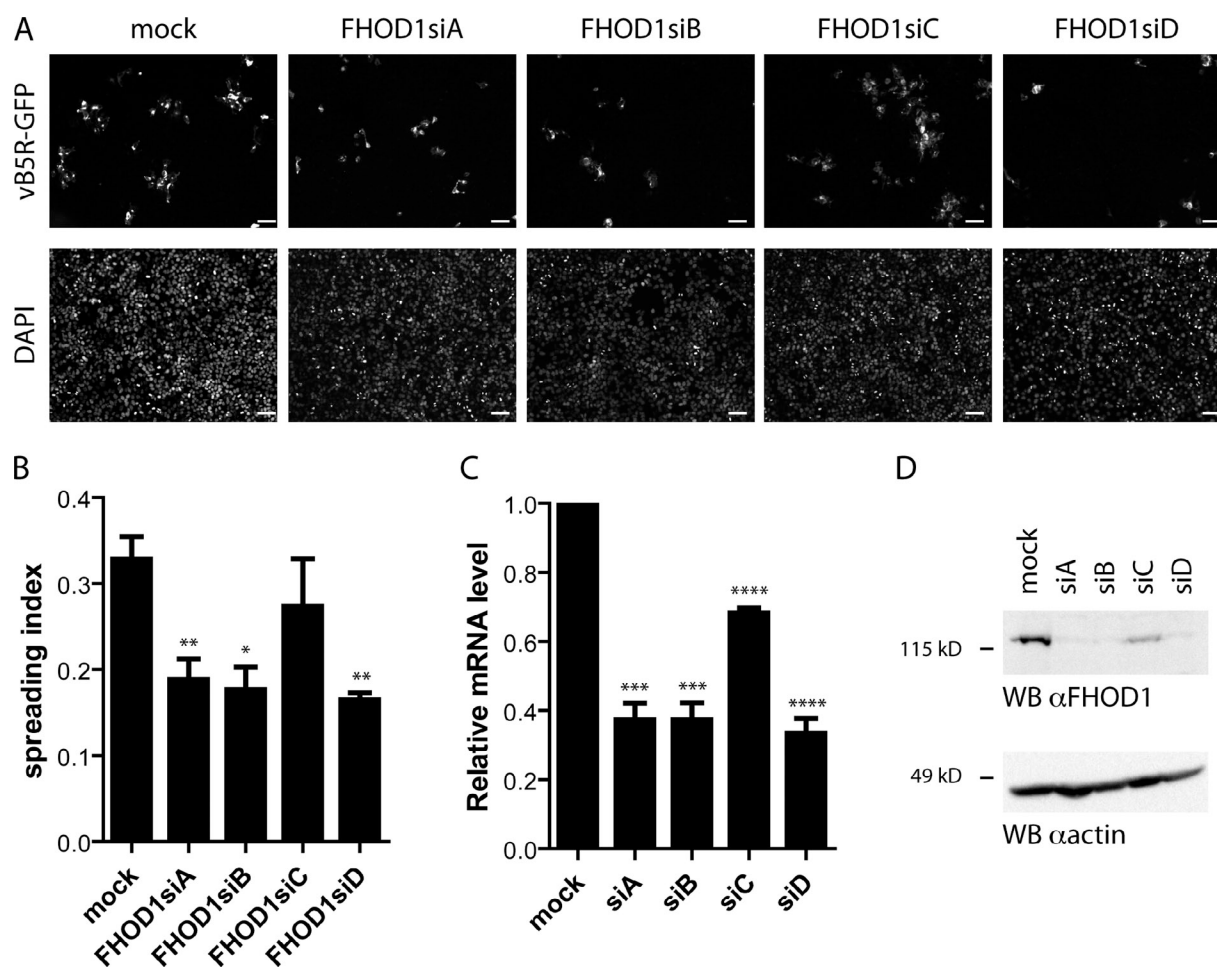
Humphries et al., 2012). Thus, the cellular requirements and related functions supporting pathogen dissemination may prove to be more complex than previously depicted.

Here, we uncover the formin FHOD1 and the small GTPase Rac1 as novel regulators of vaccinia actin tail formation. Our work suggests that vaccinia virus has evolved a complex strategy of actin-based motility relying on the integration of the activity of the ARP2/3 complex and the formin FHOD1.

Results

The formin FHOD1 is required for vaccinia virus dissemination

We identified the formin FHOD1 as a cellular factor required for vaccinia dissemination by conducting the following genetic approach. We first developed an assay for quantification of virus spread in human epithelial cells using automated fluorescence microscopy and computer-assisted image analysis. Wild-type virus expressing a B5R-GFP chimera spread from primary infected cells to neighboring cells at 16 h after infection (Fig. 1, A and B, vB5R-GFP and control). This time point was selected on the basis of preliminary time course experiments indicating that at16 h after infection, vaccinia dissemination mainly relied on ARP2/3-dependent actin-based motility (Fig. S1 A http://www.jcb.org/cgi/content/full/jcb.201303055/DC1). As

Figure 2. **The formin FHOD1 is required for vaccinia virus dissemination.** (A) Representative images of HeLa cells (nuclei, bottom) mock treated or depleted of FHOD1 using four independent siRNA duplexes targeting FHOD1 expression (FHOD1siA–D) and infected with wild-type vaccinia virus expressing GFP (vB5R-GFP, top). Bars, 100 µm. (B) The spreading index was determined as described in Fig. 1. Data are presented as the mean ± SD of three independent experiments. *, P < 0.05; **, P < 0.01; P = 0.0091 for FHOD1siA; P = 0.0150 for FHOD1siB; and P = 0.0039 for FHOD1siD, compared with the mock. (C and D) Silencing efficiency. Cells were transfected with individual FHOD1 siRNA duplexes (siA, siB, siC, and siD) and the levels of transcripts (C) and protein (D) were compared with the levels detected in mock-treated cells (mock). Data for the levels of transcripts are presented as the mean ± SD of three independent experiments. ***, P = 0.0002 for siA and siB; ****, P < 0.0001 for siC and siD, compared with the mock.
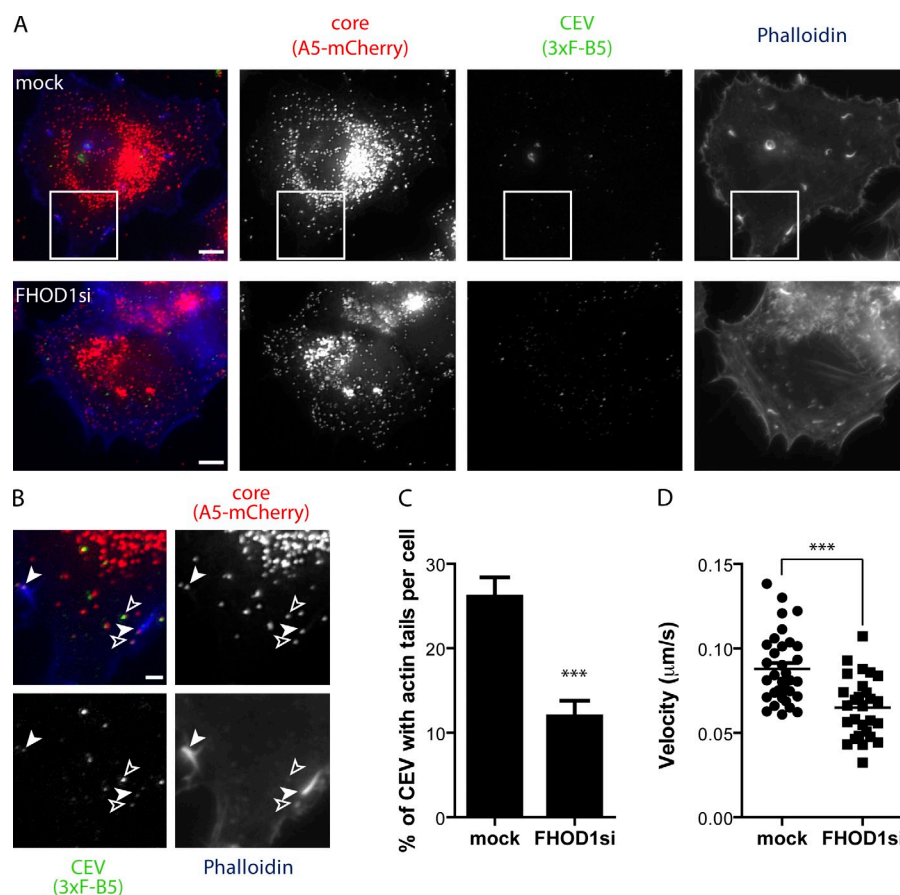
expected, the recombinant ΔA36R vaccinia variant deficient in actin tail formation led to the formation of infection foci of small size, reflecting a severe spreading defect (Fig. 1, A and B, ΔA36R). We used computer-assisted image analysis to quantify the size of the formed foci (Fig. 1 A, bottom). The vast majority of the foci formed in cells infected with the ΔA36R vaccinia variant displayed a size corresponding to single infected cells, which we defined as small (Fig. 1, ΔA36R, green). We also observed foci significantly larger in size that presumably resulted from the merge of two or more small foci (Fig. 1, ΔA36R, white). In cells infected with wild-type viruses, we observed a mixed population of foci whose size ranged from small, as defined by the size of the foci formed in cells infected with the ΔA36R vaccinia variant, to large (Fig. 1, control, green and white). To implement automated image analysis procedures, we computed the spreading index as the ratio [total foci − small foci]/[total foci], which accurately reflected the observed enrichment in foci of large size within the population of foci formed in cells infected with wild-type virus (Fig. S1 B). Statistical

analyses showed that the mean spreading index was 0.36 ± 0.08 for the wild-type virus and 0.13 ± 0.03 for the ΔA36R variant, reflecting highly significant differences in the spreading ability of the two viral strains (Fig. 1 B). We next determined whether our assay would allow us to identify host factors involved in cell-to-cell spread by silencing the expression of N-WASP and ARPC4. ARPC4 is a component of the ARP2/3 complex and N-WASP is the nucleation-promoting factor that recruits and activates the ARP2/3 complex beneath CEVs. As expected, and similar to the deletion of A36R, depletion of N-WASP or ARPC4 resulted in impaired actin-based motility, as reflected by spreading indexes of 0.13 ± 0.03 and 0.17 ± 0.05, respectively (Fig. 1, A and C).

We then assembled a siRNA library covering regulators of the actin cytoskeleton (Siripala and Welch, 2007). The screening of this library using the assay described in Fig. 1 led to the identification of FHOD1 as a cytoskeleton factor required for vaccinia virus dissemination. We validated the specific involvement of FHOD1 by using four independent silencing reagents

Figure 3. **FHOD1 stimulates actin tail initiation and elongation.** (A) Representative images of HeLa cells infected with vA5L-mCherry/3xF-B5R recombinant vaccinia virus. FLAG staining without permeabilization (green channel) was followed by permeabilization and staining of actin tails with phalloidin (blue channel). Individual CEVs were identified by colocalization of A5-mCherry signal (red channel) and FLAG staining (green channel). Bars, 10 µm. (B) Split channel images of the boxed area of the mock-treated cell images. Closed arrowheads indicate CEVs that display actin tails. Open arrowheads indicate CEVs that do not display actin tails. Bar, 3 µm. (C) Quantification of CEVs displaying actin tails in mock-treated (mock) or FHOD1-depleted (FHOD1si) HeLa cells. (D) Quantification of vaccinia virus velocity in mock-treated (mock) or FHOD1-depleted (FHOD1si) HeLa cells. Data are presented as the mean ± SEM. ***, P < 0.0001.

targeting FHOD1 expression (Fig. 2, A and B, FHOD1siA–D). We found that siRNA duplexes A, B, and D conferred the best silencing efficiency at the transcriptional level (Fig. 2 C) as well as the translational level (Fig. 2 D). These siRNA duplexes also conferred the best spreading defect phenotypes (Fig. 2, A and B). We further showed that treatment with FHOD1 siRNA duplexes did not confer general cell growth defect (Fig. S2 A). Finally, we established that FHOD1-depleted cells could support the dissemination of unrelated pathogens, such as *L. monocytogenes* (Fig. S2 B). Altogether, these results indicate that the formin FHOD1 is specifically required for vaccinia virus dissemination.
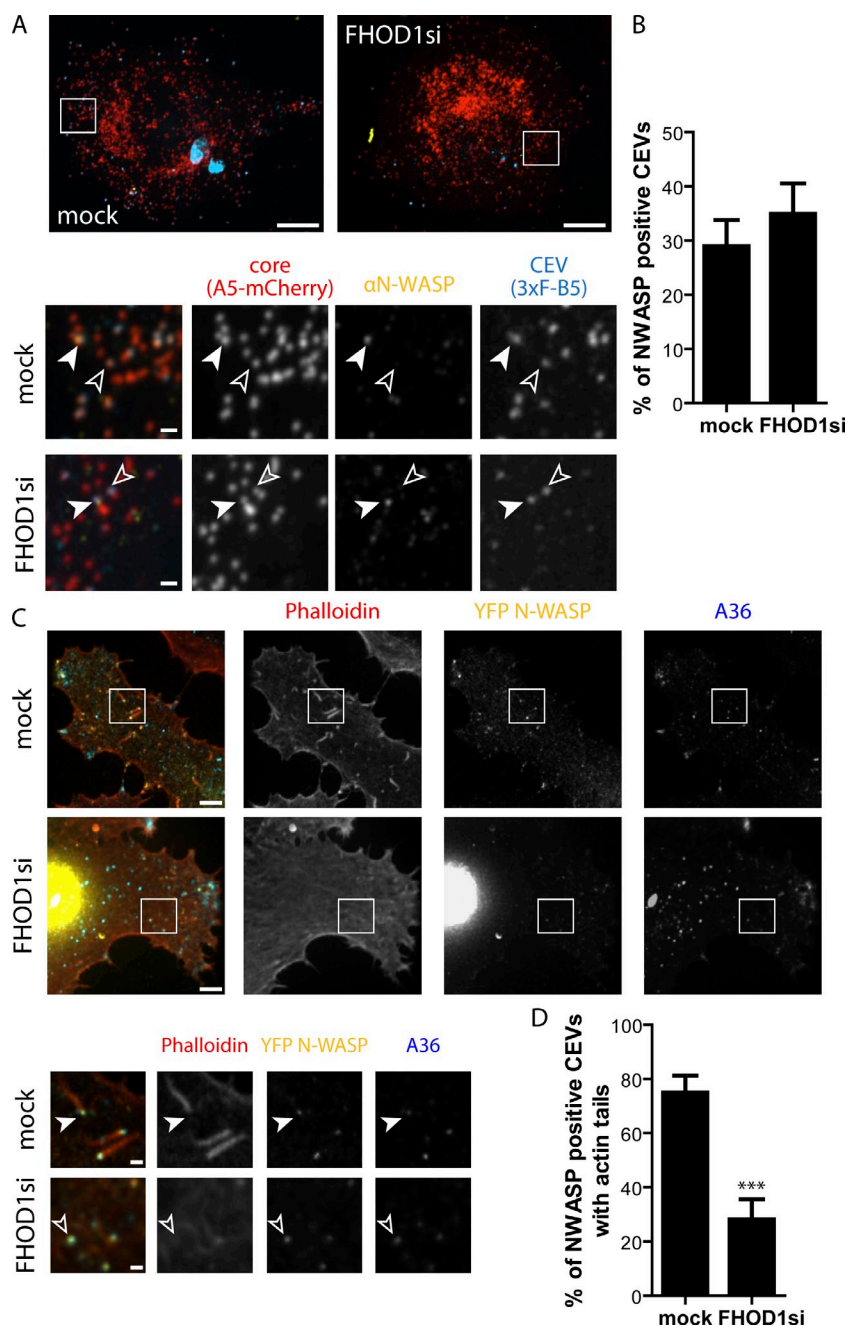
FHOD1 stimulates actin tail initiation and elongation

We next determined whether the dissemination defect observed in FHOD1-depleted cells originated from a defect in actin-based motility. To this end, we infected cells with a recombinant vaccinia virus variant expressing an mCherry-tagged version of the viral core protein A5L and a triple FLAG–tagged version of B5R (vA5L-mCherry/3xF-B5R; Alvarez and Agaisse, 2012). FLAG immunostaining without permeabilization was used to detect and quantify the number of CEVs displaying actin tails. We found that depletion of FHOD1 resulted in a 2.5-fold decrease in the number of CEVs displaying actin tails (Fig. 3, A–C). We also used time-lapse microscopy to monitor vaccinia virus actin–based motility in cells expressing YFP-N-WASP and CFP-actin. The velocity of N-WASP–tipped actin tails was determined in mock-treated or FHOD1-depleted cells. We found that silencing

FHOD1 resulted in a 30% decrease in the speed of the virus compared with mock-treated cells (Fig. 3 D). Collectively, these observations indicate that FHOD1 contributes to the initiation and the elongation of vaccinia virus actin tails.

FHOD1 is not required for N-WASP recruitment

We next determined whether the decrease in actin tail formation observed in FHOD1-depleted cells reflected a defect in the recruitment of N-WASP beneath CEVs. To this end, we analyzed endogenous N-WASP localization in cells infected with the recombinant vA5L-mCherry/3xF-B5R vaccinia variant (Fig. 4 A). We found that, in FHOD1-depleted cells, N-WASP was recruited to CEVs as efficiently as in mock-treated cells (Fig. 4 B). Because we previously observed a 2.5-fold decrease in actin tail formation in FHOD1-depleted cells (Fig. 3 C), these results suggested that, as opposed to the situation observed in mock-treated cells, a significant proportion of CEVs successfully recruited N-WASP and yet did not display actin tails in FHOD1-depleted cells. To further confirm this possibility, we quantified the number of N-WASP–positive (A36-positive) CEVs displaying actin tails in mock-treated and FHOD1-depleted cells (Fig. 4 C). We found that >75% and <25% of N-WASP–positive CEVs were associated with actin tails in mock-treated and FHOD1-depleted cells, respectively (Fig. 4 D). These results indicate that FHOD1 is not required for the recruitment of N-WASP to CEVs, but contributes to the efficiency of N-WASP–dependent actin tail formation.

Figure 4. **FHOD1 is not required for N-WASP recruitment.** (A) Representative images of HeLa cells infected with vA5L-mCherry/3xF-B5R recombinant vaccinia virus (top). Bars, 10 µm. FLAG staining without permeabilization (blue channel) was followed by permeabilization and staining of N-WASP (yellow channel). Individual CEVs were identified by colocalization of A5L-mCherry signal (red channel) and FLAG staining. Bottom panels correspond to split channel images of the boxed area of the mock-treated or FHOD1-depleted cell images (top). Closed arrowheads indicate CEVs that are positive for N-WASP localization. Open arrowheads indicate CEVs that are negative for N-WASP. Bars, 1 µm. (B) Quantification of N-WASP recruitment to CEV. Data are presented as the mean ± SEM. (C) Representative images of HeLa cells expressing YFP–N-WASP (yellow channel) infected with WR strain of vaccinia virus. Bars, 5 µm. Vaccinia virus was stained with an anti-A36 antibody (blue channel) and actin tails with phalloidin (red channel). Bottom panels correspond to split channel images of the boxed area of the mock-treated or FHOD1-depleted cell images (top). Co-localization of A36 and N-WASP was used to identify CEVs. Viruses colocalizing with N-WASP in mock-treated or FHOD1-depleted cells were scored as positive (closed arrowheads) or negative (open arrowheads) for actin tail formation. Bars, 1 µm. (D) Quantification of N-WASP–positive CEVs displaying actin tails in mock-treated or FHOD1-depleted cells. Data are presented as the mean ± SEM. ***, P < 0.0001.
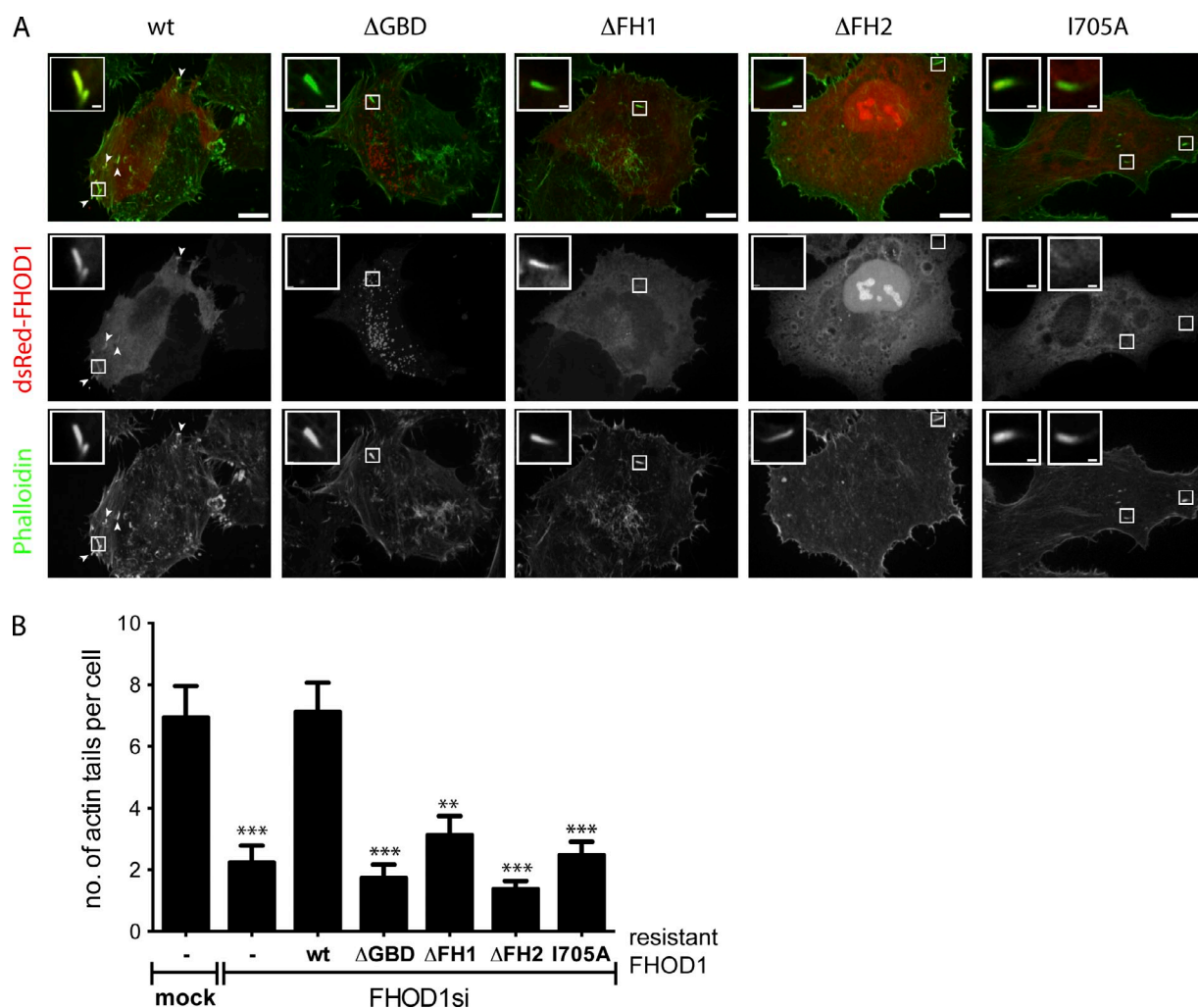
FHOD1 localizes to vaccinia actin tails

We next analyzed the localization of FHOD1 in virus-induced actin tails. Immunostaining of endogenous FHOD1 revealed co-localization with virus-tipped actin tails in infected cells (Fig. S3 A). To evaluate the specificity of FHOD1 recruitment to actin tails, we analyzed the localization of FHOD1 and mDia1 in vaccinia-infected cells. Both FHOD1 and mDia1 belong to the group of diaphanous related formins and share a similar functional domain organization. Cells expressing GFP-FHOD1 or GFP-mDia1 were infected with vaccinia virus and actin tails were scored positive or negative for the corresponding GFP fusion proteins. We observed that >90% of vaccinia virus actin tails were positive for FHOD1, whereas <25% of the tails were positive for mDia1 (Fig. S3 B). These results indicate that FHOD1 specifically localizes to vaccinia actin tails.

Functional domains of FHOD1 required for vaccinia actin tail formation

We next investigated the determinants supporting FHOD1 actin tail localization. The formin FHOD1 is organized into an N-terminal GTPase binding domain (GBD), the diaphanous autoregulatory domain (DAD) recognition domain FH3, a short proline-rich FH1 domain, an FH2 domain, and the C-terminal DAD (Schulte et al., 2008). The FH2 domain confers to formins the ability to nucleate, elongate, and cap actin filaments at barbed ends (Watanabe et al., 1999; Pruyne et al., 2002; Li and Higgs, 2003; Harris et al., 2004; Moseley et al., 2004, 2006; Otomo et al., 2005). These barbed end activities rely on a conserved isoleucine residue within the FH2 domain (isoleucine 705 in FHOD1; Harris et al., 2006). The FH1 domain is required for binding profilin-actin and may also interact with SH3
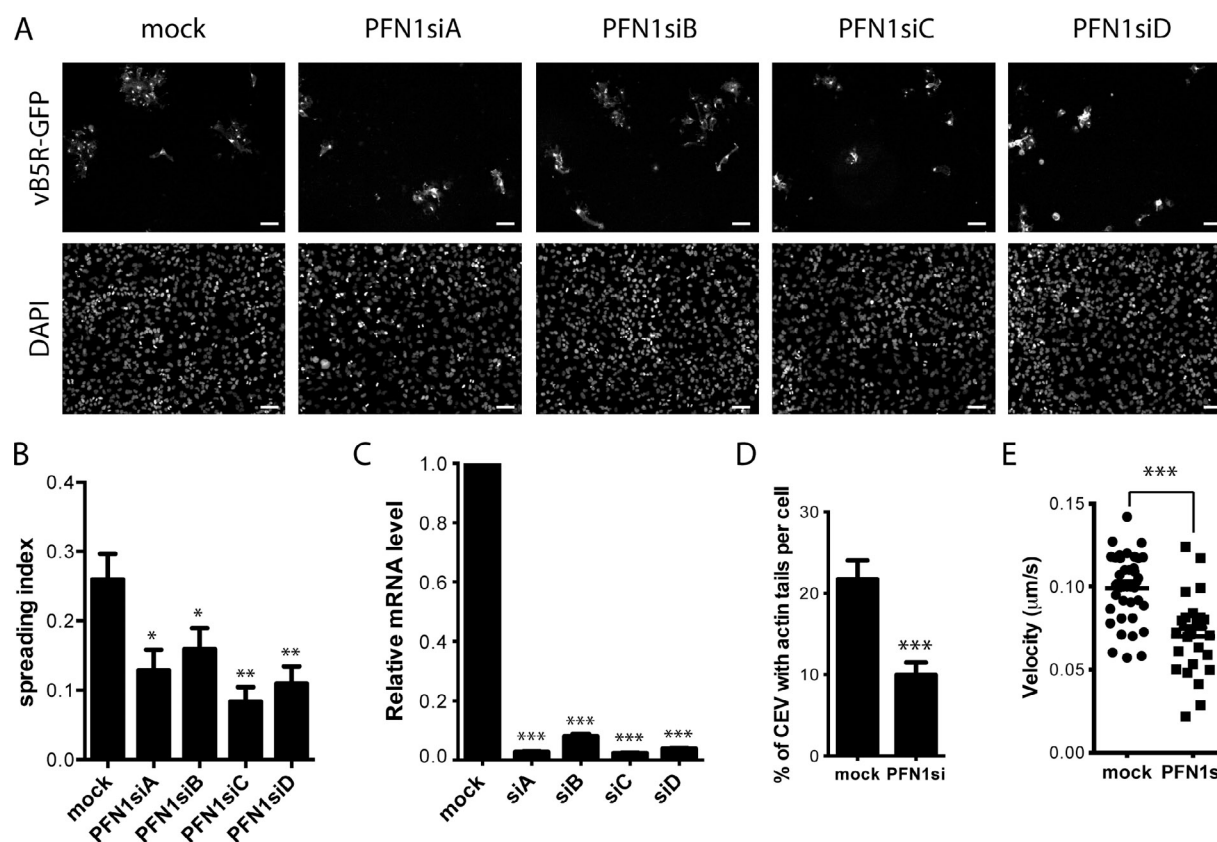
Figure 5. **FHOD1 domains required for efficient actin tail formation.** (A) Representative images of FHOD1-depleted cells expressing different silencing-resistant FHOD1 cDNA variants and infected with the WR strain of vaccinia virus. Actin tails were stained with phalloidin (green channel) and the FHOD1 cDNA variants were fused to dsRed (red channel). Bars, 10 µm. Insets show representative actin tails for FHOD1-depleted cells transfected with siRNA-resistant wild-type, ΔGBD, ΔFH1, ΔFH2, or I705A variants of FHOD1. Bars, 1 µm. Arrowheads in the panels corresponding to transfection of the full-length variant of FHOD1 (wt) indicate localization of FHOD1 to actin tails. (B) Quantitative analysis of the number of actin tails per cell in mock-treated cells (mock, –), FHOD1-depleted cells (FHOD1si, –), or FHOD1-depleted cells expressing the different FHOD1 cDNA variants (FHOD1si, resistant FHOD1 wt, ΔGBD, ΔFH1, ΔFH2, or I705A). Data are presented as the mean ± SEM. ***, $P < 0.0001$, compared with control (mock, –); **, $P = 0.0043$, for cells expressing the ΔFH1 variant (FHOD1si, ΔFH1).

or WW domain–containing proteins (Pring et al., 2003; Romero et al., 2004). Interaction between FH3 and DAD domains folds formins into an autoinhibited conformation (Alberts, 2001; Lammers et al., 2005; Nezami et al., 2006; Schönichen et al., 2006). Binding of small GTPases of the Rho/Rac/Cdc42 family to the GBD domain relieves the autoinhibited conformation and leads to formin activation (Wallar and Alberts, 2003). It has been previously shown that FHOD1 activity requires intact GBD, FH1, and FH2 domains (Takeya and Sumimoto, 2003; Schulte et al., 2008). To further characterize the role of the functional domains of FHOD1 in the formation of vaccinia virus actin tail formation, we first generated a full-length siRNA-resistant form of FHOD1 fused to dsRed. We showed that expression of this siRNA-resistant form of FHOD1 (Fig. 5, A and B, FHOD1si, wt) rescued the actin tail formation defect observed in FHOD1-depleted cells (Fig. 5, A and B, FHOD1si, –). We next determined whether siRNA-resistant forms of FHOD1,

bearing deletions of the GBD, FH1, or FH2 domains, or the I705A substitution within the FH2 domain could rescue actin tail formation in FHOD1-depleted cells. We found that the FHOD1 variant lacking the GBD domain was distributed in the cytoplasm and also in cytoplasmic vesicles in infected cells. This protein did not localize to the formed actin tails and failed to rescue the actin tail formation defect observed in FHOD1-depleted cells (Fig. 5, A and B, FHOD1si, ΔGBD). Expression of the FH1 deletion mutant showed localization to the formed actin tails (Fig. 5, A and B, FHOD1si, ΔFH1). However, this variant failed to rescue actin tail formation (Fig. 5, A and B, FHOD1si, ΔFH1). Finally, the expression of the variant carrying a deletion of the FH2 domain did not localize to the formed actin tails and, as expected, failed to rescue actin tail formation (Fig. 5, A and B, FHOD1si, ΔFH2). Similarly, the I705A substitution within the FH2 domain of FHOD1 failed to rescue actin tail formation. However, we noticed that 60% of the formed

Figure 6. **Profilin 1 stimulates actin tail initiation and elongation.** (A) Representative images of HeLa cells (nuclei, bottom) mock treated or depleted of Profilin 1 (PFN1) using four independent siRNA duplexes targeting PFN1 expression (PFN1siA–D) and infected with wild-type vaccinia virus expressing GFP (vB5R-GFP, top). Bars, 100 μm. (B) The spreading index was determined as described in Fig. 1. Data are presented as the mean ± SD of three independent experiments. *, $P < 0.05$; **, $P < 0.01$; $P = 0.0194$ for PFN1siA; $P = 0.0417$ for PFN1siB; $P = 0.0040$ for PFN1siC; and $P = 0.0093$ for PFN1siD, compared with the mock. (C) Silencing efficiency. Cells were transfected with individual PFN1 siRNA duplexes (siA, siB, siC, and siD) and were compared with mock-treated cells (mock) for silencing efficiency at the transcript level. (D) Quantification of CEVs displaying actin tails in mock-treated (mock) or PFN1-depleted (PFN1si) HeLa cells. Data are presented as the mean ± SEM. (E) Quantification of CEV actin-based motility. Data are presented as the mean ± SEM. ***, $P < 0.0001$.

actin tails displayed this mutant version of FHOD1 (Fig. 5, A and B, FHOD1si, I705A). Altogether, these results indicate that the functional domains of the formin FHOD1 are required for vaccinia actin tail formation.

Profilin-1 promotes the initiation and the elongation of vaccinia actin tails
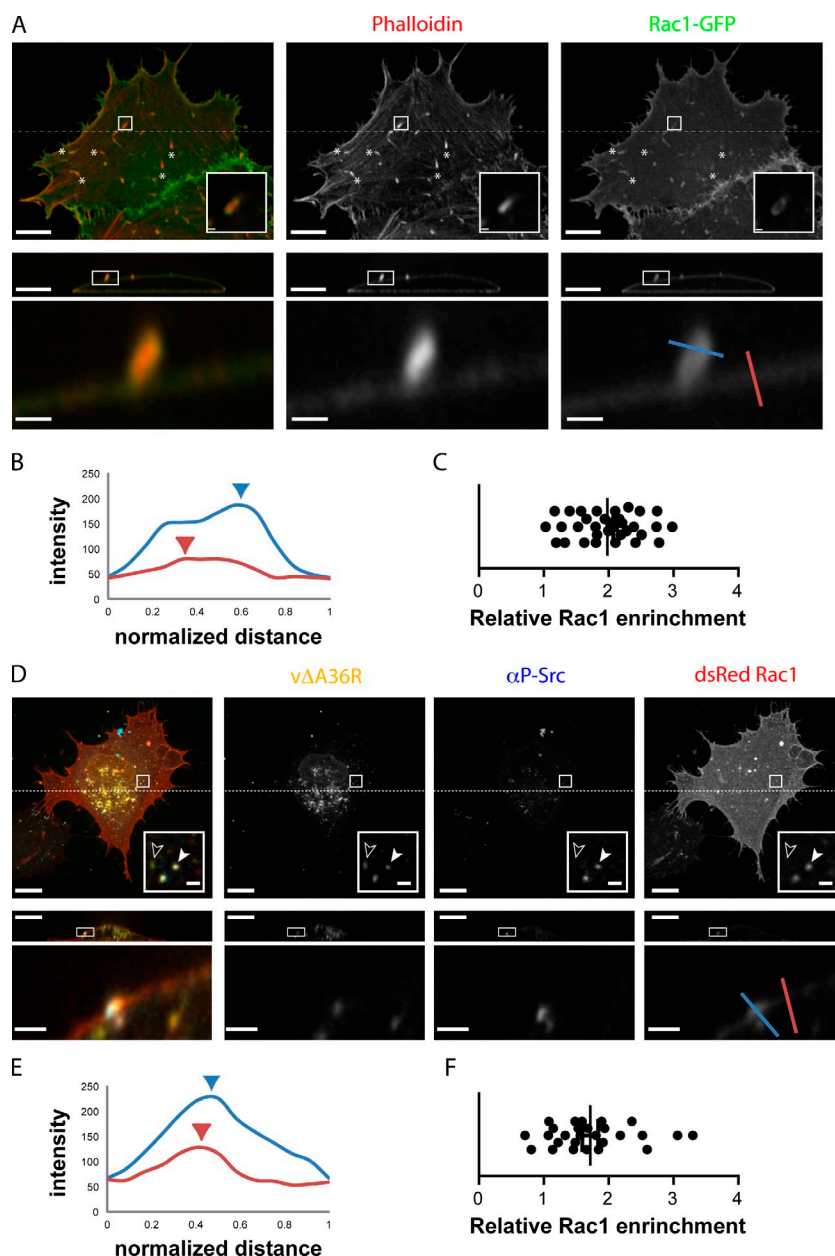
Our results indicated a role for the FH1 domain of FHOD1 in vaccinia actin tail formation, suggesting that binding of profilin-actin to the FH1 domain of FHOD1 might be required for FHOD1 function in actin tail formation. To investigate this possibility, we first analyzed the role of Profilin-1 (PFN1) in vaccinia dissemination by using the spreading assay presented in Fig. 1. Using four independent siRNA duplexes targeting PFN1 expression, we found that PFN1 depletion impaired vaccinia dissemination (Fig. 6, A and B, PFN1siA–D). The efficiency of the silencing reagents was confirmed at the transcriptional level (Fig. 6 C). To determine whether the observed spreading defect was related to a defect in actin tail formation, we quantified the number of CEVs displaying actin tails in mock-treated and PFN1-depleted cells. PFN1 depletion resulted in a 2.5-fold decrease in the number of CEVs with actin tails (Fig. 6 D). In addition, we recorded a 30% decrease in the speed of the viruses

forming actin tails in PFN1-depleted cells (Fig. 6 E). In support of the specific role of PFN1 in vaccinia actin tail formation, *L. monocytogenes* displayed wild-type motility in PFN1-depleted cells (Serio et al., 2010; unpublished data). Altogether, these observations suggest that PFN1 specifically contributes to vaccinia dissemination through the initiation and the elongation of vaccinia actin tails.

Rac1 is enriched in the membrane surrounding actin tails

Our previous results indicated a role for the GBD domain in FHOD1 actin tail localization, suggesting a potential role for Rho/Rac/Cdc42 family members in vaccinia dissemination. Imaging cells expressing GFP-tagged versions of the small GTPases showed that Rac1-GFP localized to the plasma membrane (Fig. 7 A) and was apparently enriched at the membrane surrounding actin tails (Fig. 7 A). In contrast, Cdc42-GFP was very weakly recruited to CEVs and Rho-GFP was not recruited at all (unpublished data). We next quantified the enrichment of Rac1-GFP at the plasma membrane surrounding actin tails. Computer-assisted image analysis of Rac1-GFP signal levels (Fig. 7 A [bottom] and B) showed that membrane projections corresponding to actin tails displayed a 100% increase compared

Figure 7. **Rac1 is enriched in the membrane surrounding actin tails.** (A) Representative confocal image of a cell expressing Rac1-GFP (green channel) infected with the WR strain of vaccinia virus. Actin tails were stained with phalloidin (red channel). Bars, 10 µm. (top) The insets show Rac1 localization at the plasma membrane surrounding actin tails. Bars, 1 µm. Asterisks indicate examples of Rac1-positive actin tails. Dashed lines indicate the Y coordinates corresponding to the XZ reconstructions shown in the middle panels. Bars, 10 µm. Bottom panels correspond to images of the boxed area showing that Rac1 is enriched around vaccinia actin tails. Bars, 1 µm. (B) Green channel intensities measured along a line crossing vaccinia actin tails (A and B, blue line) or crossing the plasma membrane adjacent to the actin tails (A and B, red line). (C) Quantification of Rac1 enrichment in the membrane surrounding actin tails. Rac1 enrichment represents the ratio between the maximum intensities for the line crossing the actin tail (B, blue arrowhead) and the line crossing the plasma membrane (B, red arrowhead). (D) Representative confocal image of a cell expressing Rac1-dsRed (dsRed Rac1, red channel) infected with the vGFP-ΔA36R variant of vaccinia virus (vΔA36R, yellow channel) and stained with a P-Src–specific antibody (P-Src, blue channel). Bars, 10 µm. (top, inset) A36R-deficient viruses positive for P-Src staining are indicated with closed arrowheads and viruses negative for P-Src staining are indicated with open arrowheads. P-Src–positive viruses showed Rac1 recruitment. Bars, 1 µm. Dashed lines indicate the Y coordinates corresponding to the XZ reconstructions shown in the middle panels. Bars, 10 µm. Bottom panels correspond to images of the boxed area showing that Rac1 is enriched beneath P-Src–positive viruses. Bars, 1 µm. (E) Red channel intensities measured along a line crossing P-Src–positive viruses (D and E, blue line) or crossing the plasma membrane adjacent to the virus (D and E, red line). (F) Quantification of Rac1 enrichment beneath P-Src–positive viruses. Rac1 enrichment represents the ratio between the maximum intensities for the line crossing a P-Src–positive virus (B, blue arrowhead) and the line crossing the plasma membrane (B, red arrowhead).

with the signal displayed locally at the plasma membrane (Fig. 7 C). Furthermore, we determined that the p21 binding domain (PBD)–PAK1 probe, which binds activated Rac1 (Hoppe and Swanson, 2004), was also enriched in vaccinia actin tails (Fig. S4). Thus, CEVs trigger signaling events at the plasma membrane that lead to the local recruitment and activation of Rac1.
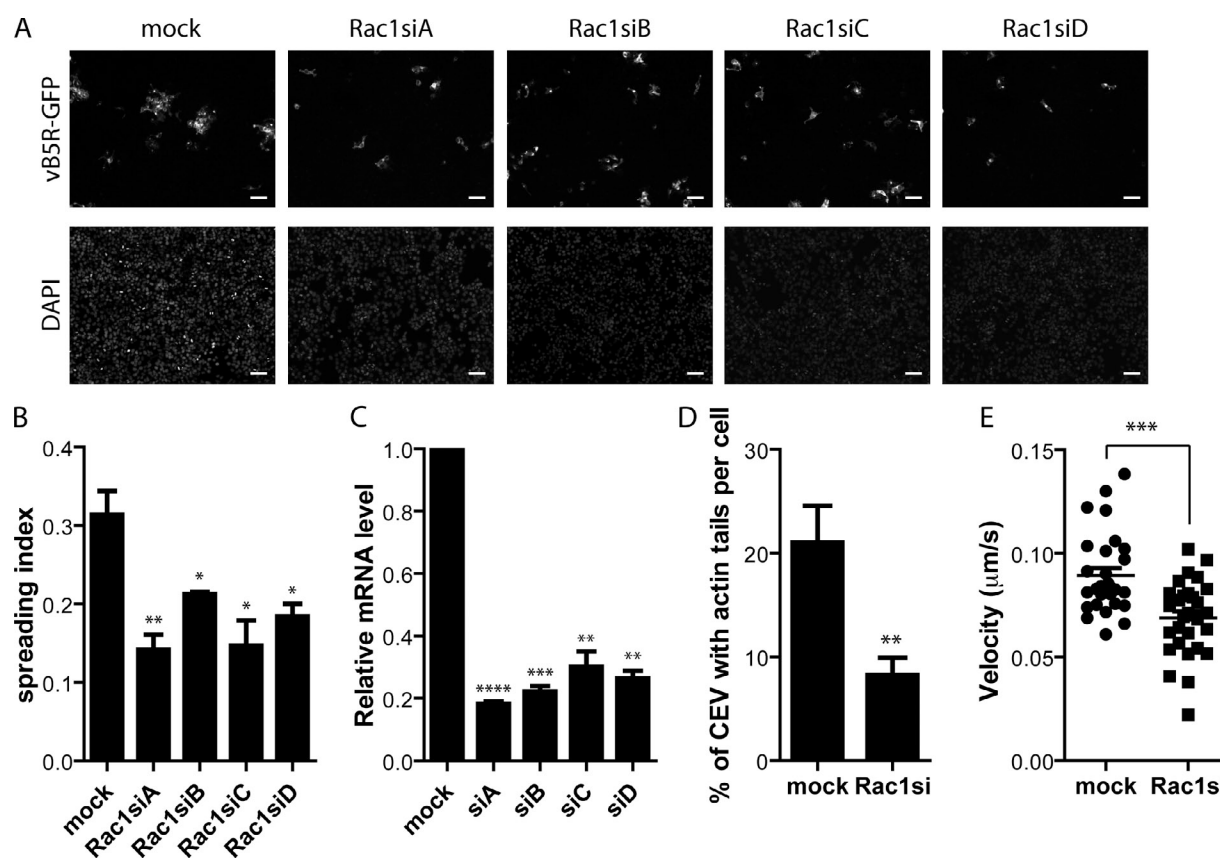
We also investigated whether Rac1 recruitment relied on the A36–N-WASP–ARP2/3 pathway. To this end we quantified Rac1 enrichment in cells infected with A36-deficient viruses (Fig. 7 D, vΔA36R). Even though vΔA36R viruses did not form actin tails, they displayed active tyrosine kinase signaling and colocalized with phosphorylated Src (Fig. 7 D, αP-Src), as previously reported for the A36R mutant defective for phosphorylation on tyrosine residues 112 and 132 (Newsome et al., 2004). Computer-assisted image analyses (Fig. 7, D [bottom] and E) revealed that the membrane located beneath A36-deficient

viruses colocalizing with phospho-Src (P-Src) displayed a 75% increase in dsRed-Rac1 signal levels compared with the levels recorded locally at the plasma membrane (Fig. 7 F). Altogether, these results indicate that signaling events triggered by CEVs at the plasma membrane lead to the A36-independent recruitment of the small GTPase Rac1.

Rac1 stimulates actin tail initiation and elongation

We next determined the functional significance of Rac1 recruitment to the plasma membrane surrounding actin tails. We first used the spreading assay presented in Fig. 1 and quantified the dissemination of vaccinia virus in Rac1-depleted cells. We found that, similar to the situation observed in FHOD1-depleted cells, vaccinia spread from cell to cell was impaired in Rac1-depleted cells (Fig. 8 A). We validated the specific involvement of Rac1 by using four independent silencing reagents targeting

Figure 8. **Rac1 stimulates actin tail initiation and elongation.** (A) Representative images of HeLa cells (nuclei, bottom) mock treated or depleted of RAC1 using four redundant siRNAs targeting Rac1 expression (Rac1siA–D) and infected with wild-type vaccinia virus expressing GFP (vB5R-GFP, top). Bars, 100 µm. (B) The spreading index was determined as described in Fig. 1. Data are presented as the mean ± SD of three independent experiments. *, P < 0.05; **, P < 0.01; P = 0.0073 for Rac1siA; P = 0.0382 for Rac1siB; P = 0.0140 for Rac1siC; and P = 0.0199 for Rac1siD, compared with the mock. (C) Silencing efficiency. Cells were transfected with individual Rac1 siRNA duplexes (siA, siB, siC, and siD) and were compared with mock-treated cells (mock) for silencing efficiency at the transcript level. Data are presented as the mean ± SD. ****, P < 0.0001; ***, P < 0.001; **, P < 0.01. P < 0.0001 for siA; P = 0.0005 for siB; P = 0.0047 for siC; and P = 0.0011 for siD, compared with the mock. (D) Quantification of CEVs displaying actin tails in mock-treated (mock) or Rac1-depleted (Rac1si) HeLa cells. Data are presented as the mean ± SEM. **, P = 0.0019. (E) Quantification of CEV actin-based motility. Data are presented as the mean ± SEM. ***, P < 0.0001.
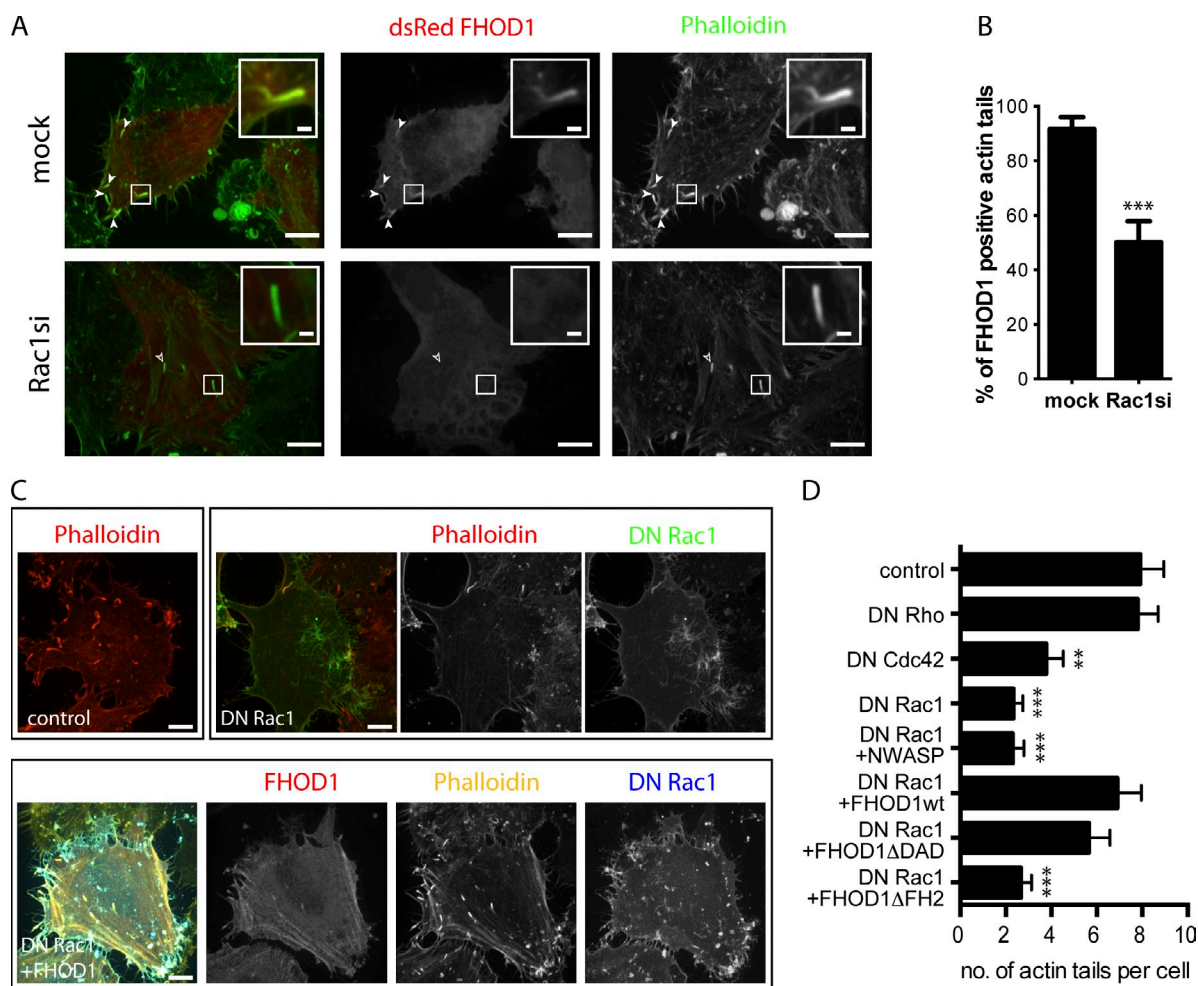
Rac1 expression (Fig. 8, A and B, Rac1siA–D). We found that all four siRNA duplexes conferred efficient silencing at the transcriptional level (Fig. 8 C). All four siRNA duplexes also conferred spreading defect phenotypes (Fig. 8, A and B). With the exception of Rac1 siRNA duplex A, treatment with Rac1 siRNA duplexes did not confer general cell growth defect (Fig. S5 A). We also established that Rac1-depleted cells supported *L. monocytogenes* spread from cell to cell (Fig. S5 B). Similar to the impact of FHOD1 depletion on actin tail formation, we found that Rac1 depletion resulted in a 2.5-fold reduction in the number of CEVs displaying actin tails and a 25% decrease in the speed of vaccinia actin-based motility (Fig. 8, D and E). Altogether, these results indicate that the small GTPase Rac1 is specifically required for vaccinia virus dissemination through stimulation of initiation and elongation of actin tails.

The localization of FHOD1 to actin tails relies on Rac1

Previous studies have established that Rac1 is specifically involved in FHOD1 activation at the plasma membrane (Westendorf, 2001; Gasteier et al., 2003; Schulte et al., 2008). Our results on vaccinia dissemination indicated that Rac1 and FHOD1 both

localized to actin tails and were required for their formation. Altogether these results led us to hypothesize that the recruitment of Rac1 to CEVs mediated the recruitment and activation of FHOD1. To test this hypothesis, we analyzed the localization of FHOD1 in Rac1-depleted cells expressing dsRed-FHOD1. We noticed that the overall level of dsRed-FHOD1 expression was systematically lower in Rac1-depleted cells, suggesting that Rac1 may regulate the overall level of FHOD1 expression through an unknown mechanism. In mock-treated and Rac1-depleted cells expressing comparable levels of dsRed-FHOD1 (Fig. 8 A), we determined that 50% of the actin tails formed in Rac1-depleted cells did not colocalize with FHOD1 (Fig. 8 B), indicating that Rac1 activity contributes to the localization of FHOD1 to actin tails.
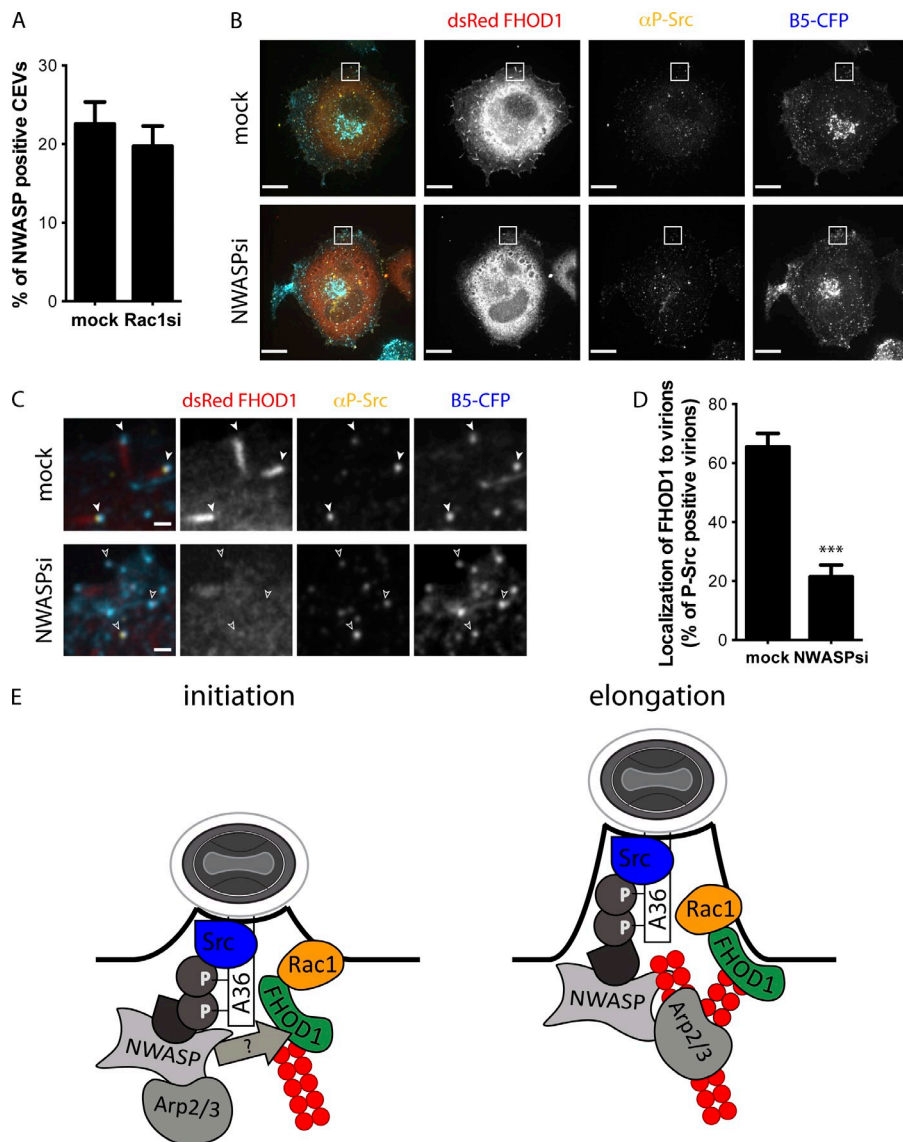
As an alternative approach and to confirm the specific role of Rac1 in FHOD1 recruitment, we used a dominant-negative version of Rac1 (Rac1N17). This construct is thought to display its dominant-negative effect through stable interaction with and titration of the guanine nucleotide exchange factors involved in Rac1 activation (Feig, 1999). We compared the effect of expressing dominant-negative versions of Rho, Cdc42, and Rac1 small GTPases on vaccinia actin tail formation. In agreement

Figure 9. **Rac1 stimulates FHOD1 recruitment to actin tails.** (A) Representative images of HeLa cells transfected with dsRed-FHOD1 and infected with WR strain of vaccinia. Bars, 10 µm. Localization of FHOD1 (red channel) to actin tails (green channel) was assessed in mock-treated (mock) or Rac1-depleted (Rac1si) cells. The inset in the top panels (mock) shows a representative actin tail decorated with FHOD1. Bars, 1 µm. Closed arrowheads indicate examples of FHOD1-positive actin tails. The inset in the bottom panels (Rac1si) shows a representative FHOD1-negative actin tail. (B) Quantitative analysis of FHOD1 localization to actin tails in mock-treated and Rac1-depleted cells. Data are presented as the mean ± SEM. ***, P < 0.0001. (C) Representative images of HeLa cells infected with the WR strain of vaccinia virus. Control cells were stained with phalloidin (red channel) to visualize actin tails. Dominant-negative Rac1 (DN Rac1) cells were transfected with GFP-Rac1 N17 (green channel) the day before infection and stained with phalloidin (red channel) to visualize actin tails. DN-Rac1 + FHOD1 cells were cotransfected with GFP-Rac1 N17 (blue channel) and dsRed-FHOD1-ΔDAD (red channel) the day before infection and stained with phalloidin (yellow channel) to visualize actin tails. Bars, 10 µm. (D) Quantitative analysis of the number of actin tails per cell in control cells (control), cells expressing dominant-negative versions of the small GTPases Rho N19 (DN-Rho), Cdc42 N17 (DN-Cdc42), and Rac1 N17 (DN-Rac1), or cells coexpressing DN-Rac1 + NWASP, DN-Rac1 + FHOD1wt, DN-Rac1 + FHOD1-ΔDAD, or DN-Rac1 + FHOD1-ΔFH2. ***, P < 0.0001, compared with control; **, P = 0.0022, for cells expressing DN-Cdc42.

with previous observations (Arakawa et al., 2007), the number of actin tails formed in cells expressing dominant-negative Rho was similar to the number observed in mock-treated cells (Fig. 9 D, control and DN Rho). In contrast, expression of dominant-negative Rac1 resulted in a threefold decrease in the number of actin tails (Fig. 9, C [top] and D [control and DN Rac1]). Expression of dominant-negative Cdc42 resulted in a twofold decrease in the number of actin tails (Fig. 9 C [top] and D [control and DN Cdc42]). Because previous studies in Cdc42 null cells (Shibata et al., 2002) and Cdc42 depletion by RNAi (unpublished data) indicated that Cdc42 is not required for vaccinia actin tail formation, these results suggested that overexpression of the dominant-negative version of Cdc42 probably affected vaccinia actin tail formation by titrating the guanine nucleotide exchange factor involved in Rac1 activation.

Interestingly, we found that overexpression of both full-length FHOD1 or a variant bearing a deletion of the C-terminal DAD domain rescued to wild-type levels the actin tail formation defects observed in cells expressing dominant-negative Rac1 (Fig. 9, C and D, DN Rac1 + FHOD1wt and DN Rac1 + FHOD1ΔDAD). As expected, overexpression of the FHOD1 variant bearing a deletion of the FH2 domain did not rescue the defect observed in cells expressing dominant-negative Rac1 (Fig. 9 D, DN Rac1 + FHOD1ΔFH2). Moreover, overexpression of components involved in the activation of the ARP2/3 complex, such as N-WASP, could not rescue actin tail formation in cells expressing DN Rac1 (Fig. 9 D, DN Rac1 and DN Rac1 + NWASP). Altogether, these results support the notion that Rac1 specifically regulates the activity of FHOD1 in vaccinia actin tail formation.

Figure 10. **N-WASP–dependent recruitment of FHOD1 and model of vaccinia actin tail initiation and elongation.** (A) Quantification of N-WASP recruitment to CEV in mock-treated and Rac1-depleted cells. Data are presented as the mean ± SEM. (B) Representative images of HeLa cells expressing dsRed-FHOD1 (red channel) infected with the vB5R-CFP variant of vaccinia virus (B5-CFP, blue channel) and stained with a P-Src–specific antibody (P-Src, yellow channel). Bars, 10 µm. (C) Split channel images of the boxed area of the mock-treated (mock) or N-WASP–depleted cells (NWASPsi) from A. Localization of FHOD1 to P-Src–positive viruses was assessed in mock-treated (mock) or N-WASP–depleted (NWASPsi) cells. Closed arrowheads indicate examples of FHOD1-positive viruses. Open arrowheads show FHOD1-negative viruses. Bars, 1 µm. (D) Quantitative analysis of FHOD1 localization to P-Src–positive viruses in mock-treated and N-WASP–depleted cells. Data are presented as the mean ± SEM. ***, P < 0.0001. (E) Model of vaccinia actin-based motility. The cytoplasmic domain of A36 is phosphorylated underneath CEVs (white and gray oval) by tyrosine kinases of the Src family leading to the recruitment of adaptor proteins (gray circles) that in turn recruit N-WASP and the ARP2/3 complex. N-WASP is required for the recruitment of FHOD1 through an unknown mechanism (left, question mark). Activation of Rac1 also contributes to the recruitment and activation of FHOD1, which may prime the formation of actin tails by nucleating the assembly of actin filaments (left). The actin filaments primed by FHOD1 are used as mother filaments by the ARP2/3 complex, which nucleates the assembly of daughter filaments (right). FHOD1 binds to the barbed ends of daughter filaments (right), as well as mother filaments (left), and increases their rate of elongation in a PFN1-dependent manner (not depicted).

The localization of FHOD1 to actin tails requires N-WASP

Our previous results suggested that, in addition to the N-WASP–ARP2/3 pathway, vaccinia virus exploits the Rac1–FHOD1 pathway for efficient actin tail formation. To further characterize the interplay between these two pathways, we quantified the recruitment of N-WASP to CEVs in Rac1-depleted cells. Similar to the results observed in FHOD1-depleted cells (Fig. 4), we found that N-WASP recruitment to CEVs was similar in mock-treated and Rac1-depleted cells (Fig. 10 A, mock and Rac1si). These results therefore indicated that the Rac1–FHOD1 pathway was not required for N-WASP recruitment. Conversely, we tested whether N-WASP may be required for FHOD1 recruitment. To this end, we infected dsRed-FHOD1–expressing cells with wild-type virus expressing a B5R-CFP chimera. We found that >70% of the viruses positive for P-Src recruited FHOD1 in mock-treated cells (Fig. 10, B–D). In contrast, <20% of P-Src–positive viruses recruited FHOD1 in N-WASP–depleted cells (Fig. 10, B–D). Collectively, our observations indicate that the localization of FHOD1 to vaccinia actin tails relies on the small GTPase Rac1 and the nucleation-promoting factor N-WASP.

Discussion

A formin in vaccinia actin tail formation

Although the central role of the ARP2/3 complex and associated regulatory proteins, such as N-WASP, has been demonstrated by unambiguous genetic approaches, it was unclear whether additional cytoskeleton regulators may also play previously unappreciated roles in vaccinia dissemination. Here, we developed high-throughput imaging and computer-assisted image analyses procedures in combination with the RNAi methodology to identify cytoskeleton factors required for vaccinia spread from cell to cell, an approach that led to the identification of a formin, FHOD1. Formin family members harbor a conserved FH2 domain that mediates barbed end activities, including nucleation, capping, and/or elongation of actin filaments. Our

results demonstrate that the FH2 domain of FHOD1 plays a critical role in the initiation and the elongation of actin tails, suggesting that FHOD1 supports vaccinia actin tail formation through nucleation and elongation of actin filaments. In further support of the role of FHOD1 through its elongation activity, we show that actin tail formation requires the FH1 domain of FHOD1 and its binding partner PFN1, which stimulates the elongation activity of formins (Romero et al., 2004; Kovar et al., 2006). We note that a recent study reported that, unlike other formin family members, FHOD1 displays capping and bundling activities, but very low elongation and no nucleation activities in vitro (Schönichen et al., 2013). Because our results strongly support the notion that FHOD1 does display nucleation and elongation activities in the context of vaccinia actin tail formation in vivo, we suggest that the apparent absence of nucleation and elongation activities observed in vitro reflects the in vivo complexity of FHOD1 regulation (see Regulation of FHOD1 activity in actin tail formation).

Respective role of FHOD1 and ARP2/3 in actin tail formation

Because FHOD1 depletion did not affect the numbers of CEVs positive for N-WASP, it is unlikely that FHOD1 regulates actin tail formation through regulation of the N-WASP–ARP2/3 pathway. Instead, our results are in agreement with the notion that, in addition to the nucleation activity displayed by the ARP2/3 complex, the nucleation activity of FHOD1 is required for efficient initiation of actin tail formation. Because the ARP2/3 complex requires mother filaments to nucleate daughter filaments, we speculate that FHOD1 primes the process of actin tail formation by nucleating the assembly of actin filaments that constitute mother filaments for the ARP2/3 complex (Fig. 10 E, left). We, however, note that the priming process is probably not absolutely required because tail formation is reduced in FHOD1-depleted cells, but not abolished. Alternatively, the decrease in the numbers of CEVs displaying actin tails may in fact reflect efficient disassembly of tails that do not elongate properly. In addition to a role in regulating actin tail initiation, our results indicate that FHOD1 also plays a role in regulating actin tail elongation. Because formins bind to the barbed ends of actin filaments and increase their rate of elongation (Romero et al., 2004; Kovar et al., 2006), our observations are therefore consistent with the notion that FHOD1 may increase the rate of actin tail elongation by increasing the rate of actin filament elongation after ARP2/3-mediated nucleation of daughter filaments (Fig. 10 E, right). Such a cooperation between the ARP2/3 complex and formins is not unprecedented and was recently described in lamellipodia for ARP2/3 and the formin FMNL2 (Block et al., 2012). In this study, the activity of the formin was regulated by the small GTPase Cdc42 at the plasma membrane and facilitated the elongation of filaments nucleated by the ARP2/3 complex. Thus, the cooperation between the ARP2/3 complex and formins constitutes an emerging theme in actin-based motility, as suggested by our present study on the role of FHOD1 in vaccinia actin tail formation.

Regulation of FHOD1 activity in actin tail formation

In addition to the expected requirement for the FH2 domain, we found that the GBD domain of FHOD1 plays an important role in vaccinia actin tail formation. The interaction between the FH3 and the DAD domains maintains formins in an autoinhibited conformation, which is relieved upon interaction of the GBD domain with activated small GTPases of the Rho family (Li and Higgs, 2003; Lammers et al., 2005). Previous studies determined that FHOD1 preferentially interacts with the small GTPase Rac1 (Gasteier et al., 2003; Schönichen et al., 2006; Schulte et al., 2008). We now provide several lines of evidence supporting the notion that Rac1 mediates vaccinia actin tail formation through the recruitment and activation of FHOD1, independently from the N-WASP–ARP2/3 pathway. We demonstrate that Rac1 is required for FHOD1 recruitment (Fig. 9), but not for N-WASP recruitment (Fig. 10). Moreover, we show that the actin tail formation defects observed in cells expressing dominant-negative Rac1 are specifically rescued by overexpression of FHOD1, but not by overexpression of a mutant version of FHOD1 lacking the FH2 domain or by overexpression of the wild-type version of N-WASP. Although Rac1 is apparently not required for N-WASP recruitment, N-WASP is nonetheless required for FHOD1 recruitment (Fig. 10 D). We speculate that adaptor proteins such as WISH, which binds FHOD1 (Westendorf and Koka, 2004) and N-WASP (Fukuoka et al., 2001), may contribute to the N-WASP–dependent recruitment of FHOD1.

Because our results indicated that Rac1 was enriched and activated at the plasma membrane surrounding vaccinia actin tails, we tested the possibility that, similar to N-WASP, the recruitment and activation of Rac1 may rely on the viral protein A36. However, P-Src–positive, A36-deficient CEVs recruited Rac1 as efficiently as wild-type viruses, indicating that Rac1 recruitment did not rely on the viral protein A36. Thus, the signaling events leading to the recruitment and activation of Rac1 beneath CEVs remain to be determined. We speculate that, in addition to mediating A36 phosphorylation, Src-mediated tyrosine kinase signaling mediates Rac1 activation, which in turn leads to the recruitment and activation of FHOD1 (Fig. 10 E). In agreement with this notion, Src was shown to regulate the activity of FHOD1 in unrelated systems (Koka et al., 2005; Hannemann et al., 2008).

In conclusion, we propose that vaccinia virus evolved the ability to display robust actin-based motility by manipulating not only the N-WASP–mediated activation of the ARP2/3 complex but also the Rac1-mediated activation of FHOD1 (Fig. 10 E).

Materials and methods

Cells and viruses

HeLa (American Type Culture Collection), HeLa S3 (American Type Culture Collection), and BS-C-1 (American Type Culture Collection) cells were grown in DMEM (Invitrogen) supplemented with 10% FBS (Gibco) at 37°C in a 5% CO_2 incubator. Vaccinia virus strains WR, vB5R-GFP (Ward and Moss, 2001b), B5R-GFP/deltaA36R (Ward and Moss, 2001a), and the B5R deletion mutant vSI-14 (Wolffe et al., 1993) were provided by B. Moss (National Institute of Allergy and Infectious Diseases, Bethesda, MD). The recombinant vA5L-mCherry/3xF-B5R virus carrying an N-terminal fusion of A5L to mCherry and a triple FLAG-tagged version of B5R was previously described (Alvarez and Agaisse, 2012). Viral strains were grown and propagated in HeLa cells and plaque assays were performed in BS-C-1 cells according to standard procedures (Earl et al., 2001). In brief, 6-well plates were seeded with 5×10^5 BS-C-1 cells per well and infected on the

next day with 10-fold serial dilutions of the virus stocks prepared in DMEM supplemented with 2.5% FBS. 2 d after infection cells were stained with 0.1% crystal violet and the virus titer was determined by plaque counting. Virus stocks were prepared from HeLa S3 cells and partially purified by centrifugation through a 36% sucrose cushion (Earl et al., 2001).

Vaccinia spreading assay
The procedure for siRNA setup in 384-well plates was described previously (Chong et al., 2011). In brief, 10 µl of individual siRNAs (200 nM) were aliquoted in 384-well plates. 10 µl of Dharmafect 1 transfection mixture (5 µl of Dharmafect 1 per 1 ml of serum-free DMEM) was dispensed per well and incubated for 20 min at room temperature. HeLa cells were lifted and resuspended at 100,000 cells/ml in DMEM supplemented with 10% FBS. 20 µl of the cell suspension were delivered to each well, and the plates were then incubated for 3 d at 37°C, in 5% CO_2. siRNA-treated cells were infected at 0.01 pfu per cell with 10 µl of a dilution of vaccinia virus vB5R-GFP stock. The plates were centrifuged at 2,000 rpm for 10 min and infection was allowed to proceed for 16 h. Infected cells were fixed in 4% paraformaldehyde in PBS and then stained with Hoechst 33348 (Molecular Probes), washed in PBS, and imaged.

High-throughput imaging and computer-assisted image analysis
384-well plates were imaged using a microscope (TE 2000; Nikon) equipped with a digital CCD camera (Orca ER; Hamamatsu Photonics), motorized stage (Prior), motorized filter wheels (Sutter Instrument), and a 10× objective (NA 0.45; Nikon) mounted on a piezo focus drive system (Physik Instrumente). Image acquisition and analyses were conducted using the MetaMorph 7.1 software (Molecular Devices). Appropriate threshold of green channel identified objects corresponding to vB5R-GFP–infected cells (Fig. S1 B, threshold). We next used the image morphometry analysis module and the dilate function in the morphology filters to generate a mask displaying foci of infection (Fig. S1 B, segmentation). This mask was used as the source image to count and classify foci of infection according to their size into large and small foci (Fig. S1 B, classifier). The spreading index was calculated as the ratio [total foci − small foci]/[total foci] for a given well.

Construction of vB5R-CFP virus
A plasmid containing B5R fused to CFP and ∼500 bp of flanking sequence on each side was constructed by excision of the ECFP ORF from pECFP-N1 (Takara Bio Inc.) with NcoI and NotI restriction enzymes and subcloning into pBMW10 (Ward and Moss, 2001b), provided by B. Ward (University of Rochester, Rochester, NY). The B5R-CFP fusion plasmid was transfected with X-tremeGENE 9 (Roche) into HeLa cells that had been infected with the vaccinia virus B5R deletion mutant vSI-14 (Wolffe et al., 1993). Recombinant viruses that formed cyan fluorescent foci were plaque purified three times. The resulting recombinant vB5R-CFP was analyzed by PCR. Primers (13) and (16) amplified a 2.3-kb DNA product in agreement with the insertion of the B5R-CFP ORF.

Silencing and validation procedures
Cells were transfected by reverse transfection with Dharmafect1 (Thermo Fisher Scientific) and individual siRNAs (50 nM final) or a pool of the four silencing reagents (12.5 nM each, 50 nM total) and were incubated for 72 h in a 24-well plate format. The sequences targeted by the individual siRNA duplexes are listed in Table S1.

For real-time PCR analysis, total RNA and first-strand cDNA synthesis was performed using the TaqMan Gene Expression Cells-to-Ct kit (Applied Biosystems), as recommended by the manufacturer, with the addition of DNaseI for the removal of unwanted genomic DNA. mRNA levels were determined by quantitative real-time PCR using the LightCycler 480 Master kit and LightCycler 480 instrument (Roche). The probes and primers were designed according to Roche recommendation.

For Western blot analysis, cells were transfected with the corresponding silencing reagents in a 24-well plate format and lysed directly in Laemmli sample buffer. The anti-FHOD1 antibody (1:1,000) was obtained from Novus Biologicals. The anti-actin antibody (1:10,000) was obtained from Sigma-Aldrich. The anti-rabbit HRP-conjugated secondary antibody (1:10,000) was obtained from Jackson ImmunoResearch Laboratories, Inc.

Immunofluorescence procedures
HeLa cells were seeded on glass coverslips, grown to 30–50% confluency, and infected with vaccinia virus at 10 pfu per cell. For vaccinia infection, cells were incubated with the virus inoculum for 1 h, and then washed three times with PBS before adding fresh media. At 10 h after infection cells

were washed with PBS, fixed in ice-cold 3% paraformaldehyde in PBS, and washed twice with PBS. To detect CEVs at the cell surface, cells infected with vA5L-mCherry/3xF-B5R were fixed and then blocked in 10% BSA/PBS, stained in 2% BSA/PBS containing mouse M2 monoclonal antibody anti-FLAG (1:1,000; Sigma-Aldrich) for 30 min, and washed five times in 2% BSA in PBS before addition of secondary antibody. To visualize actin tails, cells were permeabilized in 0.1% Triton X-100 in PBS and stained with phalloidin. Actin tails were identified as bright objects in the phalloidin staining and were required to be at least 2 µm long. To quantify localization of N-WASP to CEVs, cells were first stained for surface FLAG, then blocked and permeabilized in 10% BSA/0.1% Triton X-100 in PBS, and stained with anti–N-WASP rabbit mAb (1:200; Cell Signaling Technology). Rabbit polyclonal antibody against A36RC (1:1,000) was provided by B. Moss. P-Src was stained with a mouse monoclonal antibody anti-P-Src (Tyr416; 1:200) obtained from EMD Millipore. Alexa Fluor secondary antibodies (1:1,000) and Alexa Fluor–conjugated phalloidin (1:500) were obtained from Invitrogen. Coverslips were mounted onto glass slides using FluoroGuard Antifade Reagent (Bio-Rad Laboratories) and imaged using a TE 2000 microscope (Nikon) equipped with a digital CCD camera (Orca ER), motorized stage, motorized filter wheels, and a 60× objective (NA 0.85; Nikon) mounted on a piezo focus drive system. Image acquisition and analysis was conducted using the MetaMorph 7.1 software. Quantitative analysis of CEV formation in cells infected with the recombinant vA5L-mCherry/3xF-B5R virus was conducted as previously described (Alvarez and Agaisse, 2012). In brief, appropriate threshold and size filtering of red channel to identify objects corresponding to virus cores expressing A5-mCherry generated a mask displaying only single virus particles. The same analysis was performed for the FLAG staining channel to identify objects corresponding to FLAG-B5–expressing CEVs. Finally we used logical AND in the arithmetic function to define and count CEVs as objects corresponding to colocalization of A5-mCherry and FLAG-B5 signals. The quantification of percentage localization with CEVs was performed by visual inspection.

Plasmid construction
The pCMV5-HA-FHOD1 construct was a gift from O. Fackler (University Hospital Heidelberg, Heidelberg, Germany; Madrid et al., 2005). Full-length FHOD1 was amplified from pCMV5-HA-FHOD1 using primers (18) and (19) and cloned into pEGFP-C1 (Takara Bio Inc.) between EcoRI and BamHI restriction sites. To generate an siRNA-resistant form of FHOD1, a PCR fragment containing silent mutations in the target sequence for FHOD1 siRNA B (Table S1) was generated by fusion of the PCR products amplified with primers EFGP C and (31) and primers (32) and (19) using pEGFP-FHOD1 as a template. This was cloned into pdsRed-C1 between XhoI and BamHI restriction sites to yield siRNA-resistant pdsRed-FHOD1. The corresponding GBD domain deletion construct was obtained by cloning the PCR product amplified with primers (58) and FHOD1rev between XhoI and HindIII restriction sites. To construct the FH1 domain deletion, the PCR products obtained with primers (32) and (55) and primers (54) and (19) were fused together and cloned into pdsRed-FHOD1 between HindIII and BamHI restriction sites. The FH2 domain deletion was generated following the same cloning strategy after fusing together the PCR products generated with primers (32) and (36) and primers (35) and (19). Similarly, the PCR products obtained using primers (32) and (71) and primers (70) and (19) were fused together to generate the Ile to Ala substitution at amino acid position 705. The deletion of amino acids 1005–1064 comprising the DAD domain was generated using primers (32) and (73).

The wild-type and dominant-negative versions of Rho, Rac, and Cdc42 cDNA were described previously (Ridley et al., 1992; Bagrodia et al., 1995; Qiu et al., 1995). Dominant-negative RhoN19, RacN17, and Cdc42N17 small GTPases carry a Thr to Asn substitution at the indicated amino acid position. The corresponding GFP fusions were expressed from pEGFP-C1 vector and were provided by J. Galán (Yale University, New Haven, CT). The dsRed-Rac1 construct was obtained by subcloning the BspEI–BamHI fragment from pEGFPC1-Rac1 (Krall et al., 2002) into pDsRed-Monomer-C1. The PBD of PAK1 was amplified by PCR using primers (66) and (67) and cloned into pdsRed-N1 between XhoI and HindIII restriction sites. N-WASP ORF was amplified from HeLa cell cDNA with primers (37) and (38) and cloned into pYFP-C1 between XhoI and EcoRI. Actin-CFP was derived from actin-GFP plasmid (Rolls et al., 1999). The oligonucleotide sequences of the primers used in this study are listed in Table S2.

Plasmid transfection
Mock- and siRNA-treated HeLa cells were seeded on glass coverslips in 24-well format on day 0. DNA constructs were transfected with X-tremeGENE

9 (Roche) on day 2. On day 3, cells were infected with vaccinia virus as described for immunofluorescence procedures, fixed, and processed for imaging using a spinning disc confocal microscope (TE2000E; Nikon).

Rac1 enrichment quantification

Cells expressing Rac1-GFP were infected with WR strain of vaccinia virus. At 10 h after infection cells were fixed and stained with phalloidin. Images were acquired on a spinning disc confocal microscope (TE2000E) and a 60× oil objective (NA 1.4) using the Volocity software (PerkinElmer). Rac1 enrichment in actin tails was quantified on XZ reconstructions of the confocal images using the line profile measurement module of the Volocity software. The Rac1 enrichment in actin tails represents the ratio between the maximum intensity value in the Rac1-GFP channel obtained from a line crossing a given actin tail and the maximum value from a line crossing the plasma membrane adjacent to the actin tail (see Fig. 6). PBD-PAK1 intensity was measured in cells coexpressing PBD-PAK1-DsRed and Rac1-GFP. The PBD-PAK1 enrichment at a given vaccinia tail or filopodium base and tip was quantified in the PBD-PAK1-DsRed channel and represents the ratio between the intensity value for PBD-PAK1 at the maximum of Rac1 intensity measured in the blue channel and the corresponding value at the adjacent plasma membrane. Rac1 enrichment for the ΔA36R virus variant was performed on samples stained for P-Src with mouse monoclonal antibody anti-P-Src (Tyr416; 1:200). Rac1 enrichment was quantified in the Rac1-DsRed channel on P-Src–positive viral particles, as described for wild-type virus.

Time-lapse video microscopy

HeLa cells were seeded on 35-mm imaging dishes (MatTek Corporation). Mock- and siRNA-treated cells were cotransfected with pYFP–N-WASP and actin CFP DNA constructs the day before infection with WR strain of vaccinia virus. Images were captured at 8–10 h after infection every 12 s on a spinning disc confocal microscope (TE2000E) using a 60× oil objective (NA 1.4) and the Volocity software. Tracking of N-WASP–tipped actin tails was performed using the tracking module of the Volocity software. N-WASP–tipped actin tails tracked to calculate mean velocity were required to be motile for at least 60 s.

Statistical analysis

Quantitative analyses were performed in three independent experiments and 30–50 cells from 20 independent images were counted for each condition. Quantifications on single viruses were performed on at least 500 objects. Data are presented as mean ± SEM) and were analyzed by Student's t test using Prism 5 (GraphPad Software).

Online supplemental material

Fig. S1 shows a time course of infection of vaccinia in control and ARPC4-depleted cells, and the computer-assisted image analysis of spreading. Fig. S2 shows that FHOD1-depleted cells support *L. monocytogenes* actin-dependent dissemination. Fig. S3 shows the specificity of the recruitment of FHOD1 to vaccinia actin tails. Fig. S4 shows the enrichment of PBD-PAK1 probe in vaccinia actin tails. Fig. S5 shows that Rac1-depleted cells support *L. monocytogenes* actin-dependent dissemination. Table S1 shows the sequences targeted by individual siRNA duplexes against FHOD1, RAC1, and PFN1. Table S2 shows the sequences of the oligonucleotides used in this study. Online supplemental material is available at http://www.jcb.org/cgi/content/full/jcb.201303055/DC1.

References

Alberts, A.S. 2001. Identification of a carboxyl-terminal diaphanous-related formin homology protein autoregulatory domain. *J. Biol. Chem.* 276:2824–2830. http://dx.doi.org/10.1074/jbc.M006205200

Alvarez, D.E., and H. Agaisse. 2012. Casein kinase 2 regulates vaccinia virus actin tail formation. *Virology.* 423:143–151. http://dx.doi.org/10.1016/j.virol.2011.12.003

Arakawa, Y., J.V. Cordeiro, and M. Way. 2007. F11L-mediated inhibition of RhoA-mDia signaling stimulates microtubule dynamics during vaccinia virus infection. *Cell Host Microbe.* 1:213–226. http://dx.doi.org/10.1016/j.chom.2007.04.007

Bagrodia, S., B. Dérijard, R.J. Davis, and R.A. Cerione. 1995. Cdc42 and PAK-mediated signaling leads to Jun kinase and p38 mitogen-activated protein kinase activation. *J. Biol. Chem.* 270:27995–27998. http://dx.doi.org/10.1074/jbc.270.47.27995

Bernardini, M.L., J. Mounier, H. d'Hauteville, M. Coquis-Rondon, and P.J. Sansonetti. 1989. Identification of icsA, a plasmid locus of *Shigella flexneri* that governs bacterial intra- and intercellular spread through interaction with F-actin. *Proc. Natl. Acad. Sci. USA.* 86:3867–3871. http://dx.doi.org/10.1073/pnas.86.10.3867

Block, J., D. Breitsprecher, S. Kühn, M. Winterhoff, F. Kage, R. Geffers, P. Duwe, J.L. Rohn, B. Baum, C. Brakebusch, et al. 2012. FMNL2 drives actin-based protrusion and migration downstream of Cdc42. *Curr. Biol.* 22:1005–1012. http://dx.doi.org/10.1016/j.cub.2012.03.064

Boujemaa-Paterski, R., E. Gouin, G. Hansen, S. Samarin, C. Le Clainche, D. Didry, P. Dehoux, P. Cossart, C. Kocks, M.F. Carlier, and D. Pantaloni. 2001. *Listeria* protein ActA mimics WASp family proteins: it activates filament barbed end branching by Arp2/3 complex. *Biochemistry.* 40:11390–11404. http://dx.doi.org/10.1021/bi010486b

Chong, R., R. Swiss, G. Briones, K.L. Stone, E.E. Gulcicek, and H. Agaisse. 2009. Regulatory mimicry in *Listeria monocytogenes* actin-based motility. *Cell Host Microbe.* 6:268–278. http://dx.doi.org/10.1016/j.chom.2009.08.006

Chong, R., R. Squires, R. Swiss, and H. Agaisse. 2011. RNAi screen reveals host cell kinases specifically involved in *Listeria monocytogenes* spread from cell to cell. *PLoS ONE.* 6:e23399. http://dx.doi.org/10.1371/journal.pone.0023399

Earl, P.L., B. Moss, L.S. Wyatt, and M.W. Carroll. 2001. Generation of recombinant vaccinia viruses. *Curr. Protoc. Mol. Biol.* Chapter 16:Unit16.17.

Engelstad, M., S.T. Howard, and G.L. Smith. 1992. A constitutively expressed vaccinia gene encodes a 42-kDa glycoprotein related to complement control factors that forms part of the extracellular virus envelope. *Virology.* 188:801–810. http://dx.doi.org/10.1016/0042-6822(92)90535-W

Feig, L.A. 1999. Tools of the trade: use of dominant-inhibitory mutants of Ras-family GTPases. *Nat. Cell Biol.* 1:E25–E27. http://dx.doi.org/10.1038/10018

Frischknecht, F., V. Moreau, S. Röttger, S. Gonfloni, I. Reckmann, G. Superti-Furga, and M. Way. 1999. Actin-based motility of vaccinia virus mimics receptor tyrosine kinase signalling. *Nature.* 401:926–929. http://dx.doi.org/10.1038/44860

Fukuoka, M., S. Suetsugu, H. Miki, K. Fukami, T. Endo, and T. Takenawa. 2001. A novel neural Wiskott-Aldrich syndrome protein (N-WASP) binding protein, WISH, induces Arp2/3 complex activation independent of Cdc42. *J. Cell Biol.* 152:471–482. http://dx.doi.org/10.1083/jcb.152.3.471

Gasteier, J.E., R. Madrid, E. Krautkrämer, S. Schröder, W. Muranyi, S. Benichou, and O.T. Fackler. 2003. Activation of the Rac-binding partner FHOD1 induces actin stress fibers via a ROCK-dependent mechanism. *J. Biol. Chem.* 278:38902–38912. http://dx.doi.org/10.1074/jbc.M306229200

Goldberg, M.B., J.A. Theriot, and P.J. Sansonetti. 1994. Regulation of surface presentation of IcsA, a *Shigella* protein essential to intracellular movement and spread, is growth phase dependent. *Infect. Immun.* 62:5664–5668.

Haglund, C.M., J.E. Choe, C.T. Skau, D.R. Kovar, and M.D. Welch. 2010. *Rickettsia* Sca2 is a bacterial formin-like mediator of actin-based motility. *Nat. Cell Biol.* 12:1057–1063. http://dx.doi.org/10.1038/ncb2109

Hannemann, S., R. Madrid, J. Stastna, T. Kitzing, J. Gasteier, A. Schönichen, J. Bouchet, A. Jimenez, M. Geyer, R. Grosse, et al. 2008. The Diaphanous-related Formin FHOD1 associates with ROCK1 and promotes Src-dependent plasma membrane blebbing. *J. Biol. Chem.* 283:27891–27903. http://dx.doi.org/10.1074/jbc.M801800200

Harris, E.S., F. Li, and H.N. Higgs. 2004. The mouse formin, FRLalpha, slows actin filament barbed end elongation, competes with capping protein, accelerates polymerization from monomers, and severs filaments. *J. Biol. Chem.* 279:20076–20087. http://dx.doi.org/10.1074/jbc.M312718200

Harris, E.S., I. Rouiller, D. Hanein, and H.N. Higgs. 2006. Mechanistic differences in actin bundling activity of two mammalian formins, FRL1 and mDia2. *J. Biol. Chem.* 281:14383–14392. http://dx.doi.org/10.1074/jbc.M510923200

Heindl, J.E., I. Saran, C.R. Yi, C.F. Lesser, and M.B. Goldberg. 2010. Requirement for formin-induced actin polymerization during spread of *Shigella flexneri*. *Infect. Immun.* 78:193–203. http://dx.doi.org/10.1128/IAI.00252-09

Hiller, G., and K. Weber. 1985. Golgi-derived membranes that contain an acylated viral polypeptide are used for vaccinia virus envelopment. *J. Virol.* 55:651–659.

Hollinshead, M., G. Rodger, H. Van Eijl, M. Law, R. Hollinshead, D.J. Vaux, and G.L. Smith. 2001. Vaccinia virus utilizes microtubules for movement to the cell surface. *J. Cell Biol.* 154:389–402. http://dx.doi.org/10.1083/jcb.200104124

Hoppe, A.D., and J.A. Swanson. 2004. Cdc42, Rac1, and Rac2 display distinct patterns of activation during phagocytosis. *Mol. Biol. Cell*. 15:3509–3519. http://dx.doi.org/10.1091/mbc.E03-11-0847

Humphries, A.C., M.P. Dodding, D.J. Barry, L.M. Collinson, C.H. Durkin, and M. Way. 2012. Clathrin potentiates vaccinia-induced actin polymerization to facilitate viral spread. *Cell Host Microbe*. 12:346–359. http://dx.doi.org/10.1016/j.chom.2012.08.002

Isaacs, S.N., E.J. Wolffe, L.G. Payne, and B. Moss. 1992. Characterization of a vaccinia virus-encoded 42-kilodalton class I membrane glycoprotein component of the extracellular virus envelope. *J. Virol.* 66:7217–7224.

Katz, E., B.M. Ward, A.S. Weisberg, and B. Moss. 2003. Mutations in the vaccinia virus A33R and B5R envelope proteins that enhance release of extracellular virions and eliminate formation of actin-containing microvilli without preventing tyrosine phosphorylation of the A36R protein. *J. Virol.* 77:12266–12275. http://dx.doi.org/10.1128/JVI.77.22.12266-12275.2003

Kleba, B., T.R. Clark, E.I. Lutter, D.W. Ellison, and T. Hackstadt. 2010. Disruption of the *Rickettsia rickettsii* Sca2 autotransporter inhibits actin-based motility. *Infect. Immun.* 78:2240–2247. http://dx.doi.org/10.1128/IAI.00100-10

Koka, S., G.T. Minick, Y. Zhou, J.J. Westendorf, and M.B. Boehm. 2005. Src regulates the activity of the mammalian formin protein FHOD1. *Biochem. Biophys. Res. Commun.* 336:1285–1291. http://dx.doi.org/10.1016/j.bbrc.2005.08.257

Kovar, D.R., E.S. Harris, R. Mahaffy, H.N. Higgs, and T.D. Pollard. 2006. Control of the assembly of ATP- and ADP-actin by formins and profilin. *Cell*. 124:423–435. http://dx.doi.org/10.1016/j.cell.2005.11.038

Krall, R., J. Sun, K.J. Pederson, and J.T. Barbieri. 2002. In vivo rho GTPase-activating protein activity of *Pseudomonas aeruginosa* cytotoxin ExoS. *Infect. Immun.* 70:360–367. http://dx.doi.org/10.1128/IAI.70.1.360-367.2002

Lammers, M., R. Rose, A. Scrima, and A. Wittinghofer. 2005. The regulation of mDia1 by autoinhibition and its release by Rho*GTP. *EMBO J.* 24:4176–4187. http://dx.doi.org/10.1038/sj.emboj.7600879

Lasa, I., E. Gouin, M. Goethals, K. Vancompernolle, V. David, J. Vandekerckhove, and P. Cossart. 1997. Identification of two regions in the N-terminal domain of ActA involved in the actin comet tail formation by *Listeria monocytogenes*. *EMBO J.* 16:1531–1540. http://dx.doi.org/10.1093/emboj/16.7.1531

Li, F., and H.N. Higgs. 2003. The mouse Formin mDia1 is a potent actin nucleation factor regulated by autoinhibition. *Curr. Biol.* 13:1335–1340. http://dx.doi.org/10.1016/S0960-9822(03)00540-2

Madrid, R., J.E. Gasteier, J. Bouchet, S. Schröder, M. Geyer, S. Benichou, and O.T. Fackler. 2005. Oligomerization of the diaphanous-related formin FHOD1 requires a coiled-coil motif critical for its cytoskeletal and transcriptional activities. *FEBS Lett.* 579:441–448. http://dx.doi.org/10.1016/j.febslet.2004.12.009

Moseley, J.B., I. Sagot, A.L. Manning, Y. Xu, M.J. Eck, D. Pellman, and B.L. Goode. 2004. A conserved mechanism for Bni1- and mDia1-induced actin assembly and dual regulation of Bni1 by Bud6 and profilin. *Mol. Biol. Cell*. 15:896–907. http://dx.doi.org/10.1091/mbc.E03-08-0621

Moseley, J.B., S. Maiti, and B.L. Goode. 2006. Formin proteins: purification and measurement of effects on actin assembly. *Methods Enzymol*. 406:215–234. http://dx.doi.org/10.1016/S0076-6879(06)06016-2

Newsome, T.P., N. Scaplehorn, and M. Way. 2004. SRC mediates a switch from microtubule- to actin-based motility of vaccinia virus. *Science*. 306:124–129. http://dx.doi.org/10.1126/science.1101509

Newsome, T.P., I. Weisswange, F. Frischknecht, and M. Way. 2006. Abl collaborates with Src family kinases to stimulate actin-based motility of vaccinia virus. *Cell. Microbiol.* 8:233–241. http://dx.doi.org/10.1111/j.1462-5822.2005.00613.x

Nezami, A.G., F. Poy, and M.J. Eck. 2006. Structure of the autoinhibitory switch in formin mDia1. *Structure*. 14:257–263. http://dx.doi.org/10.1016/j.str.2005.12.003

Otomo, T., D.R. Tomchick, C. Otomo, S.C. Panchal, M. Machius, and M.K. Rosen. 2005. Structural basis of actin filament nucleation and processive capping by a formin homology 2 domain. *Nature*. 433:488–494. http://dx.doi.org/10.1038/nature03251

Parkinson, J.E., and G.L. Smith. 1994. Vaccinia virus gene A36R encodes a M(r) 43-50 K protein on the surface of extracellular enveloped virus. *Virology*. 204:376–390. http://dx.doi.org/10.1006/viro.1994.1542

Pollard, T.D., and G.G. Borisy. 2003. Cellular motility driven by assembly and disassembly of actin filaments. *Cell*. 112:453–465. http://dx.doi.org/10.1016/S0092-8674(03)00120-X

Pring, M., M. Evangelista, C. Boone, C. Yang, and S.H. Zigmond. 2003. Mechanism of formin-induced nucleation of actin filaments. *Biochemistry*. 42:486–496. http://dx.doi.org/10.1021/bi026520j

Pruyne, D., M. Evangelista, C. Yang, E. Bi, S. Zigmond, A. Bretscher, and C. Boone. 2002. Role of formins in actin assembly: nucleation and

barbed-end association. *Science*. 297:612–615. http://dx.doi.org/10.1126/science.1072309

Qiu, R.G., J. Chen, F. McCormick, and M. Symons. 1995. A role for Rho in Ras transformation. *Proc. Natl. Acad. Sci. USA*. 92:11781–11785. http://dx.doi.org/10.1073/pnas.92.25.11781

Ridley, A.J., H.F. Paterson, C.L. Johnston, D. Diekmann, and A. Hall. 1992. The small GTP-binding protein rac regulates growth factor-induced membrane ruffling. *Cell*. 70:401–410. http://dx.doi.org/10.1016/0092-8674(92)90164-8

Rietdorf, J., A. Ploubidou, I. Reckmann, A. Holmström, F. Frischknecht, M. Zettl, T. Zimmermann, and M. Way. 2001. Kinesin-dependent movement on microtubules precedes actin-based motility of vaccinia virus. *Nat. Cell Biol.* 3:992–1000. http://dx.doi.org/10.1038/ncb1101-992

Roberts, K.L., and G.L. Smith. 2008. Vaccinia virus morphogenesis and dissemination. *Trends Microbiol.* 16:472–479. http://dx.doi.org/10.1016/j.tim.2008.07.009

Rolls, M.M., P.A. Stein, S.S. Taylor, E. Ha, F. McKeon, and T.A. Rapoport. 1999. A visual screen of a GFP-fusion library identifies a new type of nuclear envelope membrane protein. *J. Cell Biol.* 146:29–44.

Romero, S., C. Le Clainche, D. Didry, C. Egile, D. Pantaloni, and M.F. Carlier. 2004. Formin is a processive motor that requires profilin to accelerate actin assembly and associated ATP hydrolysis. *Cell*. 119:419–429. http://dx.doi.org/10.1016/j.cell.2004.09.039

Röttger, S., F. Frischknecht, I. Reckmann, G.L. Smith, and M. Way. 1999. Interactions between vaccinia virus IEV membrane proteins and their roles in IEV assembly and actin tail formation. *J. Virol.* 73:2863–2875.

Sanderson, C.M., F. Frischknecht, M. Way, M. Hollinshead, and G.L. Smith. 1998. Roles of vaccinia virus EEV-specific proteins in intracellular actin tail formation and low pH-induced cell-cell fusion. *J. Gen. Virol.* 79:1415–1425.

Scaplehorn, N., A. Holmström, V. Moreau, F. Frischknecht, I. Reckmann, and M. Way. 2002. Grb2 and Nck act cooperatively to promote actin-based motility of vaccinia virus. *Curr. Biol.* 12:740–745. http://dx.doi.org/10.1016/S0960-9822(02)00812-6

Schmelz, M., B. Sodeik, M. Ericsson, E.J. Wolffe, H. Shida, G. Hiller, and G. Griffiths. 1994. Assembly of vaccinia virus: the second wrapping cisterna is derived from the trans Golgi network. *J. Virol.* 68:130–147.

Schönichen, A., M. Alexander, J.E. Gasteier, F.E. Cuesta, O.T. Fackler, and M. Geyer. 2006. Biochemical characterization of the diaphanous autoregulatory interaction in the formin homology protein FHOD1. *J. Biol. Chem.* 281:5084–5093. http://dx.doi.org/10.1074/jbc.M509226200

Schönichen, A., H.G. Mannherz, E. Behrmann, A.J. Mazur, S. Kühn, U. Silván, C.A. Schoenenberger, O.T. Fackler, S. Raunser, L. Dehmelt, and M. Geyer. 2013. FHOD1 is a combined actin filament capping and bundling factor that selectively associates with actin arcs and stress fibers. *J. Cell Sci.* 126:1891–1901. http://dx.doi.org/10.1242/jcs.126706

Schulte, A., B. Stolp, A. Schönichen, O. Pylypenko, A. Rak, O.T. Fackler, and M. Geyer. 2008. The human formin FHOD1 contains a bipartite structure of FH3 and GTPase-binding domains required for activation. *Structure*. 16:1313–1323. http://dx.doi.org/10.1016/j.str.2008.06.008

Serio, A.W., R.L. Jeng, C.M. Haglund, S.C. Reed, and M.D. Welch. 2010. Defining a core set of actin cytoskeletal proteins critical for actin-based motility of *Rickettsia*. *Cell Host Microbe*. 7:388–398. http://dx.doi.org/10.1016/j.chom.2010.04.008

Shibata, T., F. Takeshima, F. Chen, F.W. Alt, and S.B. Snapper. 2002. Cdc42 facilitates invasion but not the actin-based motility of *Shigella*. *Curr. Biol.* 12:341–345. http://dx.doi.org/10.1016/S0960-9822(02)00689-9

Siripala, A.D., and M.D. Welch. 2007. SnapShot: actin regulators I. *Cell*. 128:626.

Skoble, J., D.A. Portnoy, and M.D. Welch. 2000. Three regions within ActA promote Arp2/3 complex-mediated actin nucleation and *Listeria monocytogenes* motility. *J. Cell Biol.* 150:527–538. http://dx.doi.org/10.1083/jcb.150.3.527

Smith, G.L., A. Vanderplasschen, and M. Law. 2002. The formation and function of extracellular enveloped vaccinia virus. *J. Gen. Virol.* 83:2915–2931.

Suzuki, T., H. Mimuro, S. Suetsugu, H. Miki, T. Takenawa, and C. Sasakawa. 2002. Neural Wiskott-Aldrich syndrome protein (N-WASP) is the specific ligand for *Shigella* VirG among the WASP family and determines the host cell type allowing actin-based spreading. *Cell. Microbiol.* 4:223–233. http://dx.doi.org/10.1046/j.1462-5822.2002.00185.x

Takeya, R., and H. Sumimoto. 2003. Fhos, a mammalian formin, directly binds to F-actin via a region N-terminal to the FH1 domain and forms a homotypic complex via the FH2 domain to promote actin fiber formation. *J. Cell Sci.* 116:4567–4575. http://dx.doi.org/10.1242/jcs.00769

Tooze, J., M. Hollinshead, B. Reis, K. Radsak, and H. Kern. 1993. Progeny vaccinia and human cytomegalovirus particles utilize early endosomal cisternae for their envelopes. *Eur. J. Cell Biol.* 60:163–178.

van Eijl, H., M. Hollinshead, and G.L. Smith. 2000. The vaccinia virus A36R protein is a type Ib membrane protein present on intracellular but not extracellular enveloped virus particles. *Virology*. 271:26–36. http://dx.doi.org/10.1006/viro.2000.0260

van Eijl, H., M. Hollinshead, G. Rodger, W.H. Zhang, and G.L. Smith. 2002. The vaccinia virus F12L protein is associated with intracellular enveloped virus particles and is required for their egress to the cell surface. *J. Gen. Virol.* 83:195–207.

Wallar, B.J., and A.S. Alberts. 2003. The formins: active scaffolds that remodel the cytoskeleton. *Trends Cell Biol.* 13:435–446. http://dx.doi.org/10.1016/S0962-8924(03)00153-3

Ward, B.M., and B. Moss. 2001a. Vaccinia virus intracellular movement is associated with microtubules and independent of actin tails. *J. Virol.* 75:11651–11663. http://dx.doi.org/10.1128/JVI.75.23.11651-11663.2001

Ward, B.M., and B. Moss. 2001b. Visualization of intracellular movement of vaccinia virus virions containing a green fluorescent protein-B5R membrane protein chimera. *J. Virol.* 75:4802–4813. http://dx.doi.org/10.1128/JVI.75.10.4802-4813.2001

Watanabe, N., T. Kato, A. Fujita, T. Ishizaki, and S. Narumiya. 1999. Cooperation between mDia1 and ROCK in Rho-induced actin reorganization. *Nat. Cell Biol.* 1:136–143. http://dx.doi.org/10.1038/11056

Weisswange, I., T.P. Newsome, S. Schleich, and M. Way. 2009. The rate of N-WASP exchange limits the extent of ARP2/3-complex-dependent actin-based motility. *Nature*. 458:87–91. http://dx.doi.org/10.1038/nature07773

Welch, M.D., J. Rosenblatt, J. Skoble, D.A. Portnoy, and T.J. Mitchison. 1998. Interaction of human Arp2/3 complex and the *Listeria monocytogenes* ActA protein in actin filament nucleation. *Science*. 281:105–108. http://dx.doi.org/10.1126/science.281.5373.105

Westendorf, J.J. 2001. The formin/diaphanous-related protein, FHOS, interacts with Rac1 and activates transcription from the serum response element. *J. Biol. Chem.* 276:46453–46459. http://dx.doi.org/10.1074/jbc.M105162200

Westendorf, J.J., and S. Koka. 2004. Identification of FHOD1-binding proteins and mechanisms of FHOD1-regulated actin dynamics. *J. Cell. Biochem.* 92:29–41. http://dx.doi.org/10.1002/jcb.20031

Wolffe, E.J., S.N. Isaacs, and B. Moss. 1993. Deletion of the vaccinia virus B5R gene encoding a 42-kilodalton membrane glycoprotein inhibits extracellular virus envelope formation and dissemination. *J. Virol.* 67:4732–4741.

Wolffe, E.J., A.S. Weisberg, and B. Moss. 1998. Role for the vaccinia virus A36R outer envelope protein in the formation of virus-tipped actin-containing microvilli and cell-to-cell virus spread. *Virology*. 244:20–26. http://dx.doi.org/10.1006/viro.1998.9103